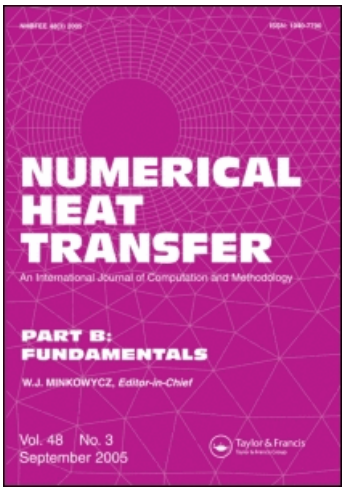

Numerical Heat Transfer, Part B: Fundamentals
Publication details, including instructions for authors and subscription information:
http://www.informaworld.com/smpp/title~content=t713723316

NONLINEAR, SUBGRID EMBEDDED FINITE-ELEMENT BASIS FOR ACCURATE, MONOTONE, STEADY CFD SOLUTIONS

Subrata Roy [a]; A. J. Baker [b]
[a] Computational Mechanics Corporation, Knoxville, Tennessee, USA [b] Mechanical & Aerospace Engineering and Engineering Science, University of Tennessee, Knoxville, Tennessee, USA

Online Publication Date: 01 March 1997

To cite this Article Roy, Subrata and Baker, A. J.(1997)'NONLINEAR, SUBGRID EMBEDDED FINITE-ELEMENT BASIS FOR ACCURATE, MONOTONE, STEADY CFD SOLUTIONS',Numerical Heat Transfer, Part B: Fundamentals,31:2,135 — 175
To link to this Article: DOI: 10.1080/10407799708915103
URL: http://dx.doi.org/10.1080/10407799708915103

NONLINEAR, SUBGRID EMBEDDED FINITE-ELEMENT BASIS FOR ACCURATE, MONOTONE, STEADY CFD SOLUTIONS

Subrata Roy
Computational Mechanics Corporation, 601 Concord St., Suite 116, Knoxville, Tennessee 37919-3382, USA

A. J. Baker
Mechanical & Aerospace Engineering and Engineering Science, University of Tennessee, Knoxville, Tennessee 37996-2030, USA

A nonlinear, subgrid embedded (SGM) finite-element basis is derived for generating accurate monotone solutions to a computational fluid dynamics (CFD) weak statement algorithm. The developed theory confirms that only the second derivative (diffusion) term is appropriate for the SGM construction, which employs element-level static condensation for efficiency and consistency. In comparison to other high-resolution methods, advantages of the SGM element formulation include arbitrary (Lagrange) embedding degree, no explicitly added artificial diffusion term, no flux limiters or switches, improved condition number for the Jacobian matrix, and excellent algorithm stability. The statically condensed SGM construction retains linear basis bandwidth, for all problem dimensions, hence exhibits no storage penalty for element or system matrices. Numerical results for 1-D, 2-D, and 3-D verification/benchmark linear and nonlinear convection-diffusion problems in steady state are presented, confirming theoretical predictions for nodally exact and monotone solutions on minimal-degree-of-freedom meshes. As a side benefit, commensurate high-order accuracy accrues to wall flux prediction on these coarse meshes, via a matrix manipulation on the weak statement algebraic construction.

INTRODUCTION

The Navier-Stokes conservation law system for state variable $q = q(x_j, t)$ is of the form

$$\mathscr{L}(q) = \frac{\partial q}{\partial t} + \frac{\partial}{\partial x_j}(\mathbf{f}_j - \mathbf{f}_j^v) - s = 0 \qquad \text{on } \Omega \times t \subset \mathscr{R}^d \times \mathscr{R}^+, 1 \leqslant j \leqslant d \quad (1)$$

where $\mathbf{f}_j = f(u_j, q)$ and $\mathbf{f}_j^v = f[\epsilon(\partial q/\partial x_j)]$ are the kinetic and dissipative flux vectors, respectively; the convection velocity is u_j; $\epsilon > 0$ is the diffusion coefficient,

Received 22 February 1996; accepted 19 August 1996.
This work was partially supported by a grant (no. MSS-9015912) from the National Science Foundation. The authors gratefully acknowledge the support provided by the UT CFD Laboratory and its corporate sponsors.

Address correspondence to Dr. A. J. Baker, Department of Mechanical and Aerospace Engineering, Engineering Science Program, University of Tennessee, 310 Perkins Hall, Knoxville, TN 37996-2030, USA. E-mail: ajbaker@cfdlab.engr.utk.edu

Numerical Heat Transfer, Part B, 31:135–175, 1997

1040–7790/97 $12.00 + .00

NOMENCLATURE

a_i	expansion coefficient	Q	discrete state variable
A	scalar constant	$r, \mathbf{r}_j, r_{ij}$	distributed SGM parameter
$c, \mathbf{c}_j$	continuum SGM parameter	R	element right of node j
d	dimension of the problem	R	statically reduced matrix
$\det_e$	transformation matrix determinant	$\{R\}$	solution residual vector
$[D_k]_e$	Lagrange diffusion matrix	$\mathscr{R}^d$	real d-dimensional space
$[D_S]_e$	SGM diffusion matrix	$\mathscr{R}^+$	temporal half-space
e	finite element	Re	Reynolds number
$f(m)$	function of m	s	source term
$\mathbf{f}_j$	kinematic flux vector	S	SGM polynomial degree
$\mathbf{f}_j^v$	viscous flux vecto	S_e	element matrix assembly operatorr
$\mathscr{F}, \mathscr{F}_{ij}$	SGM (correlation) function	t	time
$\{FQ\}$	Newton residual vector	u_j, U	velocity vector
g, g_i	SGM element embedding function	$[U]_e$	convection matrix
$\{G\}$	nodally distributed SGM vector	$\|U\|$	absolute value of velocity U
h, h_e, h_{ij}	finite-element length measure	V_e	volume (area) of a finite element
[JAC]	Jacobian matrix	x_j	spatial coordinates
k	Lagrange polynomial degree	α	SGM polynomial function of c
L	element left of node j	α, β, χ	coefficients in assembly stencil
$\mathscr{L}$	partial differential equation operator	γ, ϕ	coefficients in assembly stencil
$[M]$	assembled mass (interpolation) matrix	δ_{ij}	Kronecker delta
$\{N_k\}$	Lagrange element basis function of degree k	Δt	computational time step
		ϵ, ϵ_i	physical diffusion coefficient
$\{N_S\}$	SGM element basis function of degree S	ζ	local normalized coordinate
		η, η_i	local natural coordinate
Pe	Peclet number	θ	implicitness parameter
q	continuum state variable	ρ	radial coordinate
$\|q\|_E$	energy seminorm of q	Ω	domain

which varies parametrically; and s is a source. Appropriate initial and boundary conditions close system (1) for the well-posed statement.

Computational difficulties occur as $\epsilon \to 0$, leading to occurrence of "thin-layer" solutions containing large gradients, e.g., boundary-layer, shock. In computational fluid dynamics (CFD), this is the natural occurrence for Reynolds number becoming large. Thereby, even though the analytical solution to (1) remains smooth, monotone, and bounded, the spatially discretized CFD solution process becomes dominated by an oscillatory error mode, leading to instability in the presence of the inherent Navier-Stokes nonlinearity in $\mathbf{f}_j$.

Thus, a persistent CFD algorithm research goal is to obtain an efficient, multidimensional "arbitrary" grid algorithm that extracts an accurate, stable, and monotone solution for (1) on a *practical mesh* for arbitrary ϵ. Stabilizing techniques such as artificial viscosity methods [1–3] and/or flux correction operations [4, 5] contain one or more arbitrary parameters. Flux vector splitting methods [6] replace parameters with switches, but solutions may still exhibit oscillations near strictly local extrema. Implementation of nonlinear correction factors called *limiters* [7] requires a relatively dense mesh for interpolation to attain an essentially nonoscillatory (ENO) solution. Finally, most of these theories are developed via

analysis on 1-D schemes, hence become theoretically tenuous in a multidimensional application.

"Intelligent" algorithms for handling solution mesh adaptation in an *automatic* manner have been examined extensively in finite-element (FE) solution-adaptive "*p* and *h-p*" forms, [8–14]. Several advantages, including "unstructured meshing," accrue to these algorithms, but at a significant cost in increased algorithm operation count and storage requirements, which can hinder achieving *practical mesh* solutions. Solution monotonicity is typically not a theoretical ingredient in these theories, and as the number of degrees of freedom (DOF) increase, especially for three dimensions, the algebraic system order increases rapidly, hence also the computer resource requirement. Numerical linear algebra efficiency issues then also become a central issue.

The development herein addresses the fundamental issue of multidimensional *practical (coarse) grid solution accuracy with monotonicity.* It is based on a newly derived, genuinely nonlinear subgrid embedded (SGM), nonhierarchical finite-element basis for use in a discrete approximation of a weak statement algorithm for (1). Recent developments in the area of subgrid-scale resolution include hierarchical (*h-p*) elements [15] and inclusion of nodeless bubble functions [16]. The current development is distinctly different from these approaches in employing strictly classical Lagrange basis methodology. This leads to the key theoretical observation that the SGM basis is applicable *only* to the dissipative flux vector term in (1) [17], hence the kinetic flux vector remains a "centered" construction for the parent strictly Galerkin weak statement. The key consistency and efficiency ingredient of the SGM element is use of *static condensation* to reduce element matrix rank to that of the linear basis for any embedded degree. This is in sharp contrast to traditional enriched basis FE/FD algorithms, since the SGM element *totally contains* matrix order escalation, hence computer resource demands.

The SGM element construction for a 1-D model form of (1) leads to a theoretical *nonlinear* monotonicity constraint via enforcement of a real eigenvalue spectrum for the algorithm stencil. Thereby, the theory predicts the optimal distribution of the SGM embedded parameter (set) on each element, hence the mesh Ω^h. The generalization to nonuniform, d-dimensional discretization leads to the potential for attainment of nodally exact monotone solutions on arbitrary meshes. In concert, a high-order-accurate wall flux prediction accrues via a DOF interchange in the weak statement matrix algebraic statement. This article develops the SGM theory and documents performance for 1-D, 2-D, and 3-D verification and benchmark problem statements, belonging to the Navier-Stokes problem class, for smooth and nonsmooth solutions including nonlinearity.

THE FE WEAK STATEMENT FORMULATION

Discretization of a weak statement involves spatial and temporal components. The finite-element (FE) spatial semidiscretization of the domain Ω of (1) employs the mesh $\Omega^h = \bigcup_e \Omega_e$, where Ω_e denotes the generic computational finite-element domain. Using superscript h to denote "spatial discretization," the FE weak

statement process for (1) defines the approximation as

$$q(\mathbf{x},t) \approx q^h(\mathbf{x},t) = \bigcup_e q_e(\mathbf{x},t) \tag{2}$$

$$q_e(\mathbf{x},t) = \{N_k(\mathbf{x})\}^T \{Q(t)\}_e \tag{3}$$

where $\{\cdot\}$ denotes a column matrix, and the FE basis set $\{N_k(\mathbf{x})\}$ typically contains Chebyshev, Lagrange, or Hermite interpolation polynomials complete to degree k, plus perhaps "bubble functions" [16]. For completeness, in one dimension the kth-degree, $1 \leqslant k \leqslant 3$, Lagrange basis function sets are

$$\{N_1\} = \begin{Bmatrix} 1-\zeta \\ \zeta \end{Bmatrix} \qquad \{N_2\} = \begin{Bmatrix} (1-\zeta)(1-2\zeta) \\ 4(1-\zeta)\zeta \\ \zeta(2\zeta-1) \end{Bmatrix}$$

$$\{N_3\} = \tfrac{9}{2}\begin{Bmatrix} (1-\zeta)\left(\zeta^2-\zeta+\frac{2}{9}\right) \\ (1-\zeta)\zeta(2-3\zeta) \\ (1-\zeta)\zeta(3\zeta-1) \\ \zeta\left(\zeta^2-\zeta+\frac{2}{9}\right) \end{Bmatrix} \tag{4}$$

where $\zeta(x) = (1+\eta)/2$ and $\eta : (-1, 1)$ is the local normalized natural coordinate.

The spatially discrete FE evaluation of the *weak statement* WS^h for (1) leads to the form

$$\begin{aligned} \mathrm{WS}^h &= S_e\left(\int_{\Omega^h}\{N_k\}\left(\frac{\partial q^h}{\partial t} + \frac{\partial}{\partial x_j}(\mathbf{f}_j - \mathbf{f}_j^v)^h - s\right) d\tau\right) \equiv \{0\} \\ &= S_e\left(\int_{\Omega^h}\{N_k\}\left(\frac{\partial q^h}{\partial t} - s\right) d\tau - \int_{\Omega^h}\frac{\partial\{N_k\}}{\partial x_j}(\mathbf{f}_j - \mathbf{f}_j^v)^h\, d\tau \right. \\ &\qquad \left. + \oint_{\partial\Omega_e \cap \partial\Omega^h}\{N_k\}(\mathbf{f}_j - \mathbf{f}_j^v)^h \hat{n}_j\, d\sigma\right) \end{aligned} \tag{5}$$

where use of the Green-Gauss divergence theorem exposes the indicated boundary fluxes on $\partial\Omega^h$, S_e symbolizes the "assembly operator" carrying local (element) matrix coefficients into the global arrays, and $d\tau$ and $d\sigma$ denote differential elements on Ω and $\partial\Omega$, respectively. The surface integral in (5) contains the (unknown) boundary fluxes Dirichlet (fixed) boundary conditions are enforced.

Independent of the dimension d of Ω, and for general forms of the flux vectors, the FE weak statement (5) always yields an ordinary differential equation (ODE) system of the form

$$\mathrm{WS}^h = [M]\{Q(t)\}' + \{R\} = \{0\} \tag{6}$$

where $\{Q(t)\}'$ denotes $d\{Q\}/dt$, which vanishes for steady state. The system square matrix $[M]$ and "residual" column matrix $\{R\}$ are formed via assembly over $\Omega^h = \bigcup \Omega_e$ of corresponding element rank matrices as

$$\begin{gathered}[M] = S_e[M_k]_e \qquad \text{and} \\ \{R\} = S_e\{R_k\}_e = S_e(([U]_e + [D]_e + [B]_e)\{Q\}_e - \{b\}_e)\end{gathered} \tag{7}$$

where subscript k in (7) emphasizes coefficient dependence on FE basis degree k in (3). On each finite element Ω_e, the contained compositions are $[D]_e$ for the dissipative flux vector $\mathbf{f}_j^p$, $[U]_e$ for the convective flux vector $\mathbf{f}_j$, and $[B]_e$ for the $(d-1)$-dimensional implementation of the boundary flux contribution; $\{b\}$ is the matrix of all known data.

The form (6) provides the statement of local time derivative necessary to evaluate a temporal Taylor series (TS). Selecting the θ-implicit one-step Euler family, then

$$\begin{aligned}\{Q(t_{n+1})\} \equiv \{Q\}_{n+1} &= \{Q\}_n + \Delta t[\theta\{Q\}'_{n+1} + (1-\theta)\{Q\}'_n] + \mathscr{O}(\Delta t^{f(\theta)}) \\ &= \{Q\}_n - \Delta t[M]^{-1}(\theta\{R\}_{n+1} + (1-\theta)\{R\}_n)\end{aligned} \tag{8}$$

where subscript n denotes time level. Clearing $[M]^{-1}$ and collecting terms to a homogeneous form yields the WS^h + θ TS algorithm terminal statement,

$$\{FQ\} = [M]\{Q_{n+1} - Q_n\} + \Delta t(\theta\{R\}_{n+1} + (1-\theta)\{R\}_n) = \{0\} \tag{9}$$

The *Newton algorithm* for solution of (9) is

$$[\text{JAC}]\{\Delta Q\}_{n+1} = -\Delta t\{R\}_n \qquad \text{linear} \tag{10a}$$

$$[\text{JAC}]\{\delta Q\}^{p+1} = -\{FQ\}^p_{n+1} \qquad \text{nonlinear} \tag{10b}$$

where, for iteration index p,

$$\{Q\}^{p+1}_{n+1} \equiv \{Q\}^p_{n+1} + \{\delta Q\}^{p+1} = \{Q\}_n + \sum_{i=1}^{p} \{\delta Q\}^{i+1} \tag{11}$$

The linear form (10a) converges in a single step, hence $\{Q\}_{n+1} = \{Q\}_n + \{\Delta Q\}_{n+1}$. In either instance, the Newton *Jacobian* is formed as

$$[\text{JAC}] = \frac{\partial\{FQ\}}{\partial\{Q\}} = [M] + \theta\Delta t\left(\frac{\partial\{R\}}{\partial\{Q\}}\right) \tag{12}$$

For the steady-state problem, $\partial/\partial t = 0$ in (1), hence clearing through the Δt in (9)–(12) yields $[\text{JAC}] = \partial\{R\}/\partial\{Q\}$ and $\{FQ\} = \{R\}$.

THE SGM FINITE ELEMENT

The global assembly of the element canonical form of the diffusion matrix $[D]_e$ resembles an identity matrix, *excellent* for numerical computation independent of the basis degree k, ([17, chap. 5.5). Conversely, the assembly of the element canonical convection matrix $[U]_e$ always yields a null matrix. In addition, in higher dimensions, the matrix $[U]_e$ cannot be statically condensed, as the convective information contained at element mid-side nodes may not be eliminated. Hence, contrary to the convective flux vector manipulation as a stability-enhancement approach, the SGM element procedure is restricted to the diffusion matrix resulting from f_j^v [17].

1-D Elements

The Lagrange linear ($k = 1$) and quadratic ($k = 2$) FE basis polynomial set, the $k = 1$, $p = 2$ hierarchical (bubble) element, and the SGM $S = 2$ ($k = 2$, reduced) Lagrange element for one dimension are compared in Figures 1*a*–1*d*. Both the Lagrange $k = 2$ and p-hierarchical elements contain an extra degree of freedom (node 2 in Figures 1*b* and 1*c*). For the SGM element, the explicit appearance of the embedded degree of freedom is eliminated via static condensation (Appendix A), a well-known FE methodology leading to the Schur compliment [18, 19].

For the linear dissipative flux vector FE construction, static condensation of any $k > 1$ basis Lagrange element in one dimension simply returns the $k = 1$ form [17]. Therefore, the SGM theory augments the diffusion matrix via an *embedding* function $g(x, c)$, hence the name "SubGrid eMbedded." The definite integral form of the SGM basis function set, denoted $\{N_S\}$, for $[D]_e$ in (7), is

$$\int_{\Omega_e} \frac{\partial\{N_S\}}{\partial x} \frac{\partial\{N_S\}^T}{\partial x}\, dx = \int_{\Omega_e} g(x,c) \frac{\partial\{N_k\}}{\partial x} \frac{\partial\{N_k\}^T}{\partial x}\, dx \Bigg|^R \tag{13}$$

where the statically condensed, reduced Rank form is denoted as $|^R$. The embedded polynomial $g(x, c)$ contains one arbitrary (at present) parameter c for each additional Lagrange degree $k \geqslant 2$. The form of the 1-D SGM element basis set $\{N_S\}$ for $k = 2 = S$ is expressed, analogous to the $k = 1$ Lagrange basis, (4), as

$$\{N_S\} = \begin{Bmatrix} 1 - \mu \\ \mu \end{Bmatrix} \qquad \text{but} \qquad \mu = \sum_{i=1}^{\infty} a_i \zeta_i^{\alpha} \tag{14}$$

In (14), μ is a polynomial function of an expansion coefficient set, a_i, dependent on embedding degree k, and the $k = 1$ element local coordinate ζ, and α is a function of c. A detailed computation of the SGM 1-D basis is provided in Appendix B.

If the embedded polynomial in (13) is selected as quadratic, then $g_2 = \{1, c, 1\}\{N_2\}$, where $\{N_2\}$ is the Lagrange quadratic basis. Then, for $S = 2 = k$, the

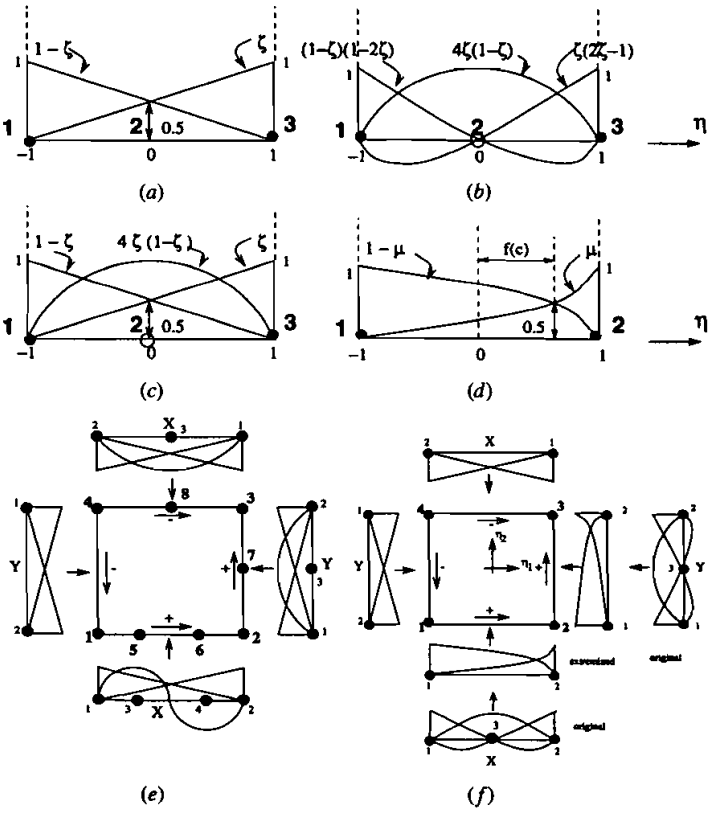

Figure 1. Comparison of standard, hierarchical, and SGM elements in one and two dimensions: (*a*) 1-D Lagrange element, $k = 1$; (*b*) 1-D Lagrange element, $k = 2$; (*c*) 1-D hierarchical element, $k = 1$, $p = 2$; (*d*) 1-D SGM Lagrange element, $k = 2$ reduced; (*e*) 2-D hierarchical p-element, $k = 1, 2, 3$ selectively; (*f*) 2-D SGM element, $S = 2$.

3×3 element matrix form for $[D]_e$ prior to condensation is

$$[D_{k=2}]_e = \frac{1}{15h_e}\begin{bmatrix} (18c + 17) & (7 - 2c) & -(16c + 24) \\ (7 - 2c) & (18c + 17) & -(16c + 24) \\ -(16c + 24) & -(16c + 24) & (32c + 48) \end{bmatrix} \tag{15}$$

Static condensation of this matrix yields

$$[D_{k=2}]_e^R \Rightarrow [D_{S=2}]_e = \frac{1}{3h_e}\begin{bmatrix} (2c + 1) & -(2c + 1) \\ -(2c + 1) & (2c + 1) \end{bmatrix} \tag{16}$$

The discussion in Appendix B confirms that $c \geqslant 1$ is the requirement. For $c \equiv 1$, $[D_{S-2}]_e$ in (16) is identical to the linear Lagrange matrix,

$$[D_{k-1}]_e = \frac{1}{h_e}\begin{bmatrix} 1 & -1 \\ -1 & 1 \end{bmatrix}$$

This degeneracy is termed *consistent*, which occurs only for $d = 1$. Specifically, for $d > 1$ dimensions, static condensation of a $k > 1$ diffusion matrix does not yield the $k = 1$ form.

In the case of distributed data in the dissipative flux vector, as might occur, for example, with eddy viscosity in a turbulent flow simulation, the base form of the element diffusion matrix is

$$[D_2]_e = \int_{\Omega_e} \{a, b\}_e \{N_1\} \frac{d\{N_2\}}{dx} \frac{d\{N_2\}^T}{dx} dx \tag{17}$$

where $\{a, b\}$ are nodal eddy viscosity and the interpolations in $[D_2]_e$ use mixed degree k. Then, for one dimension and $S = 2$, for example, the SGM base definition upon static condensation is

$$[D_2]_e = \frac{1}{3(a+b)_e h_e}\begin{bmatrix} (a^2+b^2+4ab)_e & -(a^2+b^2+4ab)_e \\ -(a^2+b^2+4ab)_e & (a^2+b^2+4ab)_e \end{bmatrix} \tag{18}$$

Note that only for $a = 1 = b$ does (18) reduce to the Lagrange linear basis matrix $[D_1]_e$. The combination of a, b, and g_2 is admissible as $\tilde{g}_2 = \{a, c, b\}\{N_2\}^T$. Thereby, the turbulent viscosity is distributed using coefficients a and b, while c remains available for an optimal selection.

2-D and 3-D SGM Finite Elements

The d-dimensional form in the dissipative flux vector diffusion matrix $[D]_e$ in (4), formed via the SGM element (denoted by subscript S), is

$$[D_S]_e \equiv \int_{\Omega_e} g(\mathbf{x}, \mathbf{c}) \frac{\partial\{N_k\}}{\partial \mathbf{x}} \frac{\partial\{N_k\}^T}{\partial \mathbf{x}} d\tau \Bigg|^R \tag{19}$$

$$= \int_{\Omega_e} \frac{\partial\{N_S\}}{\partial \mathbf{x}} \frac{\partial\{N_S\}^T}{\partial \mathbf{x}} d\tau \tag{20}$$

and many selections are possible. For $d \geqslant 1$, $g_2(\mathbf{x}, \mathbf{c})$ is written as

$$g_2 = \{G\}_e^T \{N_2\} \tag{21}$$

For the $d = 2$ vector $\mathbf{c} = (c_x, c_y)$, the element array is $\{G\}_e^T = \{1, 1, 1, 1, c_x, c_y, c_x, c_y, c_x c_y\}$ and $\{N_2\}$ is the corresponding Lagrange quadratic basis set. The array $\{G\}_e$ may be represented by the matrix outer product

$$\{G\}^T \Rightarrow \{1, c_x, 1\} \otimes \{1, c_y, 1\} \tag{22}$$

hence is pictured as the tensor product $A \otimes B$ of $A = \{1, c_x, 1\}$ and $B = \{1, c_y, 1\}$, that is,

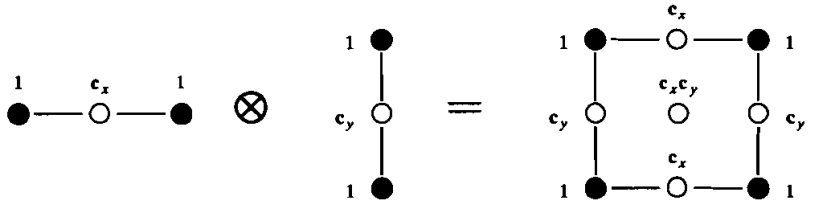

The $d = 3$ extension is obvious. Element constructions for $d = 2$ are illustrated in Figures 1*e* and 1*f*. Figure 1*e* graphs a p-hierarchical 2-D element with two quadratic sides ($p = 2$), one cubic side ($p = 3$), and a linear side. The $k = 2$ ($S = 2$) condensed 2-D SGM element, graphed in Figure 1*f*, is very distinct from both the p-element and the Lagrange $k = 2$ element.

The diffusive flux vector matrix $[D]_e$ in (4), formed with the Lagrange bilinear ($k = 1$) basis in two dimensions for a generic Cartesian element of unit span, is

$$[D_1]_e = \int_{\Omega_e} \nabla\{N_1\} \cdot \nabla\{N_1\}^T \, d\tau = \frac{\det_e}{6} \begin{bmatrix} 4 & -1 & -2 & -1 \\ -1 & 4 & -1 & -2 \\ -2 & -1 & 4 & -1 \\ -1 & -2 & -1 & 4 \end{bmatrix} \tag{23}$$

where $\det_e$ is the transformation matrix determinant, equal to one-fourth the plane area of Ω_e. The $S = 2$ extremized form for (19) for two dimensions is constructed as

$$[D_S]_e = \frac{\det_e}{6} \begin{bmatrix} d_{11} & d_{12} & d_{13} & d_{14} \\ d_{21} & d_{22} & d_{23} & d_{24} \\ d_{31} & d_{32} & d_{33} & d_{34} \\ d_{41} & d_{42} & d_{43} & d_{44} \end{bmatrix} \tag{24}$$

where each matrix element d_{ij} in (24) is a distinct polynomial function of c_x and c_y (Appendix C). Assuming that $c_x = c = c_y$, the first term in (24) becomes

$$d_{11} = \frac{2c + 1}{15(148c^2 + 164c + 73)}(656c^3 + 2{,}032c^2 + 1{,}838c + 549) \tag{25}$$

Simplifying further to $c_x = c_y = c = 1$, the $S = 2$ SGM diffusion matrix form is

$$[D_S]_e = \frac{\det_e}{66}\begin{bmatrix} 29 & -11 & -7 & -11 \\ -11 & 29 & -11 & -7 \\ -7 & -11 & 29 & -11 \\ -11 & -7 & -11 & 29 \end{bmatrix} \tag{26}$$

The distinctions between (23) and (26) are apparent.

STABILITY, MONOTONICITY, EIGENVALUE SPECTRUM

An eigenvalue analysis of an algorithm stencil is used classically for determining stability. For the algorithm algebraic system $[A]\{Q\} = \{b\}$, the solution vector $\{Q\}$ is nonoscillatory (monotone) only if the eigenvalues of $[A]$ are devoid of an imaginary component. Furthermore, if the real parts of these eigenvalues are non-negative, then the solution is stable.

The general assembled stencil at node j for a finite-element discretization with $[D]_e$ is

$$\cdots + \hat{\alpha}Q_{j-2} + \hat{\beta}Q_{j-1} + \hat{\gamma}Q_j + \hat{\beta}Q_{j+1} + \hat{\alpha}Q_{j+2} + \cdots = 0 \tag{27}$$

In comparison, for a uniform 1-D discretization with node spacing h, the set of higher-order compact finite-difference (FD) schemes for the diffusion term in (1) is expression as [20]

$$\begin{aligned} \phi\frac{d^2q_{j-2}}{dx^2} + \chi\frac{d^2q_{j-1}}{dx^2} + \frac{d^2q_j}{dx^2} + \chi\frac{d^2q_{j+1}}{dx^2} + \phi\frac{d^2q_{j+2}}{dx^2} \\ = \alpha\frac{Q_{j+1} - 2Q_j + Q_{j-1}}{h^2} + \beta\frac{Q_{j+2} - 2Q_j + Q_{j-2}}{4h^2} \\ + \gamma\frac{Q_{j+3} - 2Q_j + Q_{j-3}}{9h^2} + \cdots \end{aligned} \tag{28}$$

Hence, any higher (than second)-order-accurate FD or FE stencil is at least pentadiagonal involving node $j \pm 2$ to describe action at node j.

The relations between the coefficients α, β, γ, and ϕ, χ in (28) determine the truncation error of the approximation. Table 1 summarizes these data. For the Lagrange basis 1-D FE assembly on a uniform mesh centered at node j, for the second derivative in (1) written as (27), the comparison determination is presented in Table 2.

The SGM condensed matrix assembly, for any embedding degree in the second derivative term in (1), always yields a constant times the $k = 1$ basis

Table 1. FD recursion coefficients α, β, γ

Truncation order	Coefficients in (28)
Third	$\alpha + \beta + \gamma = 1 + 2\chi + 2\phi$
Fifth	$\alpha + 2^2\beta + 3^2\gamma = \frac{4!}{2!}(\chi + 2^2\phi)$
Seventh	$\alpha + 2^4\beta + 3^4\gamma = \frac{6!}{4!}(\chi + 2^4\phi)$
Ninth	$\alpha + 2^6\beta + 3^6\gamma = \frac{8!}{6!}(\chi + 2^6\phi)$
Eleventh	$\alpha + 2^8\beta + 3^8\gamma = \frac{10!}{8!}(\chi + 2^8\phi)$

tridiagonal stencil, i.e.,

$$\frac{d^2q_j}{dx^2} \approx \alpha_S \frac{Q_{j+1} - 2Q_j + Q_{j-1}}{h} \tag{29}$$

where $\alpha_S = (2c + 1)/3$ for $k = 2$ embedding g_2. Thus, for $S = 2$, FE weak statement algorithm (6) for the 1-D steady convection-diffusion form of (1) with no source ($s = 0$), assembled at node j for notation $Q_j = Q(jh)$, yields the recursion

$$\frac{(2c + 1)\epsilon}{3h}[-Q_{j-1} + 2Q_j - Q_{j+1}] + \frac{U}{2}[-Q_{j-1} + Q_{j+1}] = 0 \tag{30}$$

On a nonuniform meshing, the stencil form is

$$-\left(\frac{(2c_L + 1)\epsilon}{3h_L} + \frac{U}{2}\right)Q_{j-1} + \left(\frac{(2c_L + 1)\epsilon}{3h_L} + \frac{(2c_R + 1)\epsilon}{3h_R}\right)Q_j$$
$$-\left(\frac{(2c_R + 1)\epsilon}{3h_R} - \frac{U}{2}\right)Q_{j+1} = 0 \tag{31}$$

where subscripts L and R denote to the "left" and "right" of node j, respectively. Finally, $S = 2$ SGM element stencil with linear embedding $g_1 = \{a, b\}_e\{N_1\}$ for

Table 2. FE recursion coefficients $\hat{\alpha}, \hat{\beta}, \hat{\gamma}$

Truncation order	Coefficients in (27)
Third	$\hat{\alpha} = -h, \hat{\beta} = 0, \hat{\gamma} = 0$
Fifth	$\hat{\alpha} = -\frac{4h}{3}, \hat{\beta} = \frac{2h}{3}, \hat{\gamma} = 0$
Seventh	$\hat{\alpha} = -\frac{63h}{40}, \hat{\beta} = \frac{9h}{5}, \hat{\gamma} = -\frac{39h}{40}$

arbitrary meshing is

$$-\left(\frac{(a_L^2 + b_L^2 + 4a_Lb_L)\epsilon}{3(a_L + b_L)h_L} + \frac{U}{2}\right)Q_{j-1}$$

$$+\left(\frac{(a_L^2 + b_L^2 + 4a_Lb_L)\epsilon}{3(a_L + b_L)h_L} + \frac{(a_R^2 + b_R^2 + 4a_Rb_R)\epsilon}{3(a_R + b_R)h_R}\right)Q_j$$

$$-\left(\frac{(a_R^2 + b_R^2 + 4a_Rb_R)\epsilon}{3(a_R + b_R)h_R} - \frac{U}{2}\right)Q_{j+1} = 0 \tag{32}$$

For the $(m + 1) \times (m + 1)$ tridiagonal matrix system assembly of the $S = 2$ SGM basis on an m uniform 1-D FE discretization (30), the eigenvalue distribution of the tridiagonal matrix stencil is [21]

$$\lambda^l = \frac{2(2c + 1)\epsilon}{3h} - 2\sqrt{\left(\frac{(2c + 1)\epsilon}{3h} + \frac{U}{2}\right)\left(\frac{(2c + 1)\epsilon}{3h} - \frac{U}{2}\right)}\cos(l\pi h)$$

$$1 \leqslant l \leqslant m \tag{33}$$

Thus, λ^l can be represented as a Pick function [21] of form $\Phi(\zeta) = \alpha(\zeta) + i\beta(\zeta)$, where $i = \sqrt{-1}$. Thereby, the FE solution of (29) will be monotone for λ^l possessing no imaginary part [22]. This is ensured by the parameter c satisfying the constraint

$$\left|\frac{(2c + 1)\epsilon}{3h}\right| \geqslant \left|\frac{U}{2}\right| \tag{34}$$

Further, for any $c \geqslant -\frac{1}{2}$ and $\epsilon > 0$, the λ^l are uniformly positive. Hence, the FE algorithm is absolutely stable for all admissible $c \geqslant 1$.

Extending to a nonuniform mesh of measure h_e, and with $U \to u_e$ a cellwise constant, for all $\epsilon > 0$, the SGM $S = 2$ solution should be strictly monotone for

$$c_e \geqslant \frac{1}{2}\left(\frac{3|u_e|h_e}{2\epsilon} - 1\right) \tag{35}$$

For the SGM linear embedding g_1, the solution is monotone, provided

$$\left|\frac{(a^2 + b^2 + 4ab)\epsilon}{3(a + b)h}\right|_e \geqslant \left|\frac{U}{2}\right| \tag{36}$$

and $(a, b)_e > 0$ by definition.

For general applications, a nodally distributed (subscript j) SGM parameter is preferable to an element parameter. Therefore, defining $r_j = (2c_j + 1)/3$, the

monotonicity constraint form (34) becomes

$$\frac{2c_j + 1}{3} \equiv r_j \geqslant \frac{|u_j|h_j}{\epsilon \mathscr{F}} = \frac{|u_j|h_j \,\mathrm{Re}}{\mathscr{F}} \tag{37}$$

where Reynolds number Re can replace ϵ and $\mathscr{F} > 0$ is a real number. In one dimension, $\mathscr{F}$ is precisely determined from the eigenvalue analysis, $\mathscr{F} = 2$ for the linear convection-diffusion (Peclet) problem, $\mathscr{F} = 6$ for the linear stationary wave solution, while $\mathscr{F} = 3$ for nonlinear convection-diffusion (viscous Burgers) equation [17]. However, for multidimensional problems, determining the exact form for $\mathscr{F}$ involves definition of a correlation function $\mathscr{F}_{ij} = f(\mathrm{Re}, \mathrm{det}_e)$, the form of which was validated using the test data of the 2-D and 3-D linear Peclet problem solutions.

For this correlation function $\mathscr{F}_{ij}$ and for velocity field $\mathbf{u}_j = (u_{1j}, u_{2j}, u_{3j})$, principal coordinate mesh measures h_{1j}, h_{2j}, and h_{3j}, and principal coordinate diffusion parameter set $\boldsymbol{\epsilon}_j \Rightarrow (\epsilon_{1j}, \epsilon_{2j}, \epsilon_{3j})$, the condition for a d-dimensional monotone solution is expressed for scalar components of $\mathbf{r}_j = (r_{1j}, r_{2j}, r_{3j})$ in (22) as

$$r_{ij} \geqslant \frac{|u_{ij}|h_{ij}}{\mathscr{F}_{ij}\epsilon_{ij}} \qquad \text{where} \qquad \mathscr{F}_{ij} = \left(\frac{AV_e}{\epsilon_{ij}^{d-1}h_{ij}}\right)^{1/d}, \; 1 \leqslant i \leqslant d, \text{ and } 1 \leqslant j \leqslant \mathrm{Nnode} \tag{38}$$

Hence, only the scalar $0 < A < 2$ remains undefined, hence must be estimated, and $V_e\,(= 2^d \,\mathrm{det}_e)$ is the volume (area) of the d-dimensional element.

RESULTS AND DISCUSSION

Computational results, verifying theory, and summarizing performance for a range of verification and benchmark problems that model the Navier-Stokes equation system are presented herein. The problem domains lie on $\mathscr{R}^d$ for $d = 1, 2, 3$ in (1), with an SGM function approximation on 1-D, 2-D, and 3-D finite elements. The following steps form the SGM element solution process.

Step 1. Use monotonicity constraint (37) or (38) to compute distributed c_j or r_j, or estimate $r_{ij} = f(|u_{ij}|, h_{ij}, \epsilon_{ij})$.

Step 2. Form

$$[D_k]_e = \int_{\Omega_e} g_2(\mathbf{c}) \frac{\partial\{N_k\}^T}{\partial x_j} \frac{\partial\{N_k\}^T}{\partial x_j} \, d\tau$$

where $g_2(\mathbf{c}) = \{G\}^T\{N_2\}$.

Step 3. Reduce $[D_k]_e$ to $[D_S]_e$ using static condensation, (70a).

Step 4. Form the weak statement WS^h (9):(71) for the discretization $\Omega^h \cup_e \Omega_e$.

Step 5. Solve (10a) or (10b), including flux computation at all Dirichlet boundary nodes.

A traditional measure for estimating semidiscrete approximation error, $e^h = q - q^h$, is the L_2 "energy seminorm" $\|\cdot\|_E$, defined as

$$\|q^h\|_E \equiv 0.5 \int_\Omega \nabla q^h \cdot \epsilon \nabla q^h \, d\tau \tag{39}$$

where ϵ remains the diffusion coefficient in the dissipative flux vector in (1). For a linear elliptic boundary-value problem, if q is the exact solution to an mth-order variational statement, hence the parent differential equation is of order $2m$, then the discrete approximation error is bounded in energy in the form [23]

$$\|e^h\|_{E(\Omega)} \leqslant C h_e^{2(k+1-m)} \|q\|^2_{H^{k+1}} \tag{40}$$

where C is a constant independent of h_e, a mesh measure, and $\|q\|_{H^{k+1}}$ is the Sobolev norm containing up to the $(k+1)$st derivative of the exact solution. Hence, for sufficiently smooth solutions, the error in the finite-element approximation, measured in energy, converges as the $2(k+1-m)$ power of a mesh measure under uniform discretization refinement.

For a 1-D axisymmetric steady conduction problem, the $S = 2\ g_1 = \{a, b\}\{N_1\}$ linear SGM form results on the radius identification, recall (17), hence $a = R_L$ and $b = R_R$, for the generic element. Conversely, the $S = 2\ g_2$ quadratic SGM with distributed parameter $c_j, r_j > 0$ is validated for all other steady linear and nonlinear convection-diffusion problem statements in one, two, and three dimensions.

Axisymmetric Steady-State Conduction

The heat conduction statement in polar coordinates is

$$-\frac{1}{\rho}\frac{d}{d\rho}\left(\rho\epsilon\frac{dq}{d\rho}\right) - s = 0 \qquad \rho_1 < \rho < \rho_2 \tag{41a}$$

$$\alpha q + \epsilon \nabla q \cdot \hat{\mathbf{n}} - \alpha q_n = 0 \qquad \rho = \rho_1, \text{ for arbitrary } \alpha \tag{41b}$$

$$q(\rho_2) = q_b \qquad \rho = \rho_2 \tag{41c}$$

The g_1 SGM form occurs naturally for this statement, for which $a = \rho_L$ and $b = \rho_R$ for the generic master element. For constant ϵ, the exact solution to (41a) is logarithmic,

$$q(\rho) = A_1 + B_1 \ln \rho \tag{42}$$

Therefore, any piecewise polynomial approximate solution will clearly exhibit error, hence quantizable solution convergence trends will exist. Figure 2 summarizes algorithm asymptotic convergence for the base Lagrange and various SGM forms of degree k, hence reduced form S. The data confirm the classical theory for $k = 1, 2$ Lagrange basis elements, as the data are logarithmically interpolated by straight lines of slope equal to $2k$. In distinction, for the g_1 embedding and $S \geqslant 2$

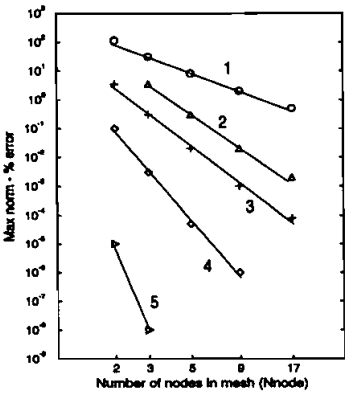

line no.	k	S	slope
1	1	0	2.0
2	2	0	4.0
3	0	2	4.5
4	0	3	6.2
5	0	4	10.8

(*a*)

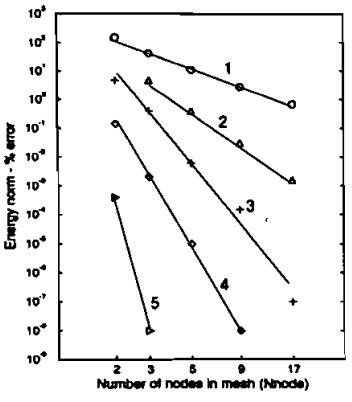

line no.	k	S	slope
1	1	0	2.0
2	2	0	4.0
3	0	2	5.5
4	0	3	6.9
5	0	4	12.6

(*b*)

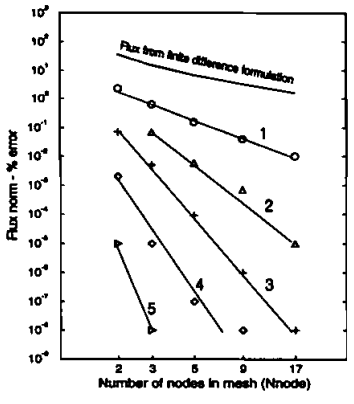

Flux from Weak Statement

line no.	k	S	slope
1	1	0	2.0
2	2	0	4.0
3	0	2	5.3
4	0	3	6.5
5	0	4	10.0

(*c*)

Figure 2. Convergence study, 1-D steady heat conduction problem: (a) Max norm; (b) energy norm; (c) flux point norm.

SGM element, the convergence rate (slope) increases rapidly as S increases. Specifically, for $S = 4$, the convergence data are interpolated by a line of slope 12.6, which exceeds the classical $k = 4$ slope of 8. Convergence rates measured in the max norm, Figure 2*a*, are somewhat lower than in energy for $S \geqslant 2$, Figure 2*b*.

For the Dirichlet boundary condition (41*c*), one can easily compute the (unknown) boundary flux via the WS^h construction. The resultant WS^h algebraic rearrangement of the Newton statement (10*a*), for direct flux computation (Appendix D) on a uniform mesh is

$$\frac{\epsilon}{h}\begin{bmatrix} 1 & -1 & & \mathbf{O} & \\ -1 & 2 & -1 & & \\ & & \ddots & & \\ & & -1 & 1 & -\Lambda \\ & \mathbf{O} & & \Lambda & \Lambda^2 \end{bmatrix}\begin{Bmatrix} Q_1 \\ Q_2 \\ \vdots \\ Q_{J-1} \\ F_J \end{Bmatrix} = \begin{Bmatrix} \alpha q_r \\ 0 \\ \vdots \\ 0 \\ Q_J \end{Bmatrix} \tag{43}$$

where $\Lambda = h/\epsilon$, for the terminal Ω_e, and F_J is the associated (unknown) normal boundary flux at the last node J.

Figure 2*c* graphs boundary flux convergence for the rearranged WS^h (43). While the $k = 2$ Lagrange FE algorithm results are significantly better than the $k = 1$ solutions, the SGM $S > 1$ boundary flux computations are at least two orders of magnitude more accurate than either Lagrange FE result and exhibit a higher convergence rate. The flux computed via any finite-difference formula is totally dependent on the mesh measure h_e, hence the associated error is up to five orders of magnitude larger than the SGM WS^h prediction on the coarsest mesh, Figure 2*c*.

Steady Conduction with Source

Consider the parabolic equation

$$\frac{1}{\rho}\frac{d}{d\rho}\left(\rho\frac{dq}{d\rho}\right) = -s \qquad 1 \leqslant \rho \leqslant 2 \tag{44}$$

where $s = s(\rho)$ is assumed linear. The generic solution to (44) is

$$q = -\frac{\rho^2}{4} + \ln \rho + b \tag{45}$$

with specific forms.

Case I: Both ends Dirichlet.

$$q|_{\rho=1} = 0 \Rightarrow b = \frac{1}{4} \qquad \text{and} \qquad q|_{\rho=2} = 0 \Rightarrow a = \frac{3}{4\ln 2}$$

Hence,

$$q = -\frac{\rho^2}{4} + \frac{3}{4}\frac{\ln \rho}{\ln 2} + \frac{1}{4}$$

Case II: Left end Dirichlet, right end homogeneous Neumann

$$q|_{\rho=1} = 0 \Rightarrow b = \frac{1}{4} \qquad \text{and} \qquad \left.\frac{dq}{d\rho}\right|_{\rho=2} = 0 \Rightarrow a = 2$$

Hence,

$$q = -\frac{\rho^2}{4} + 2\ln\rho + \frac{1}{4}$$

The corresponding matrix statement (6) is $S_e(\{\rho\}_e^T[D_S]_e\{Q\}_e - \{\rho\}_e^T[M_k]_e\{S\}_e) = \{0\}$, where $\{\rho\}_e$ contains the nodally discretized values of radius ρ and $[M_k]_e$ are the corresponding FE *hypermatrices* [19]. The locally extremized SGM element is as given earlier. For the linear embedding $g_1 = \{\rho_L, \rho_R\}\{N_1\}^T$, the resulting change in the data structure is readily illustrated. On element $e = 1$, choosing the linear basis for $[D_k]_e$ yields

$$[D_k]_{e=1} = \begin{bmatrix} 3.5 & -3.5 \\ -3.5 & 3.5 \end{bmatrix} \tag{46}$$

In comparison, using the $k = 2$ basis function for $[D_k]$ and the corresponding data $\{\rho\}_{e=1}^T \equiv \{1, \frac{7}{6}, \frac{4}{3}\}$, and then reducing the square matrix $\{\rho\}_e^T[D_2]_e$ via (70*a*) yields

$$[D_S]_{e=1} = \begin{bmatrix} 3.47619049 & -3.47619049 \\ -3.47619049 & 3.47619049 \end{bmatrix} \tag{47}$$

For a four-node uniform mesh, the S-embedded ($S \geqslant 1$) solution comparison details are summarized in Figure 3. These results clearly confirm a sharp decrease in error as S goes from 1 to 2. Conversely, for $S > 2$, increasing S does not significantly affect the solution (error), Figures 3*a*, 3*c*, and 3*e*–3*f*. Convergence comparison in energy between the standard linear basis FE ($k = 1$) and the combination h-S solutions is graphed in Figures 3*b* and 3*d*. These results indicate that the convergence slope increases significantly as the (h-S) combination spans (12, 2) to (48, 4). Specifically, the solution error trend confirms selection of $S = 2$ as essentially optimal for improved solution accuracy and computational efficiency.

Steady "Peclet" Problem, $d = 1$

The governing parabolic convection-diffusion equation is

$$\frac{d}{dx}\left(uq - \epsilon\frac{dq}{dx}\right) = 0 \qquad \text{on } 0 \leqslant x \leqslant \ell \tag{48}$$

which upon nondimensionalization and for constant u becomes

$$\frac{d}{dx}\left(q - \frac{1}{\text{Pe}}\frac{dq}{dx}\right) = 0 \qquad \text{on } 0 \leqslant x \leqslant 1 \tag{49}$$

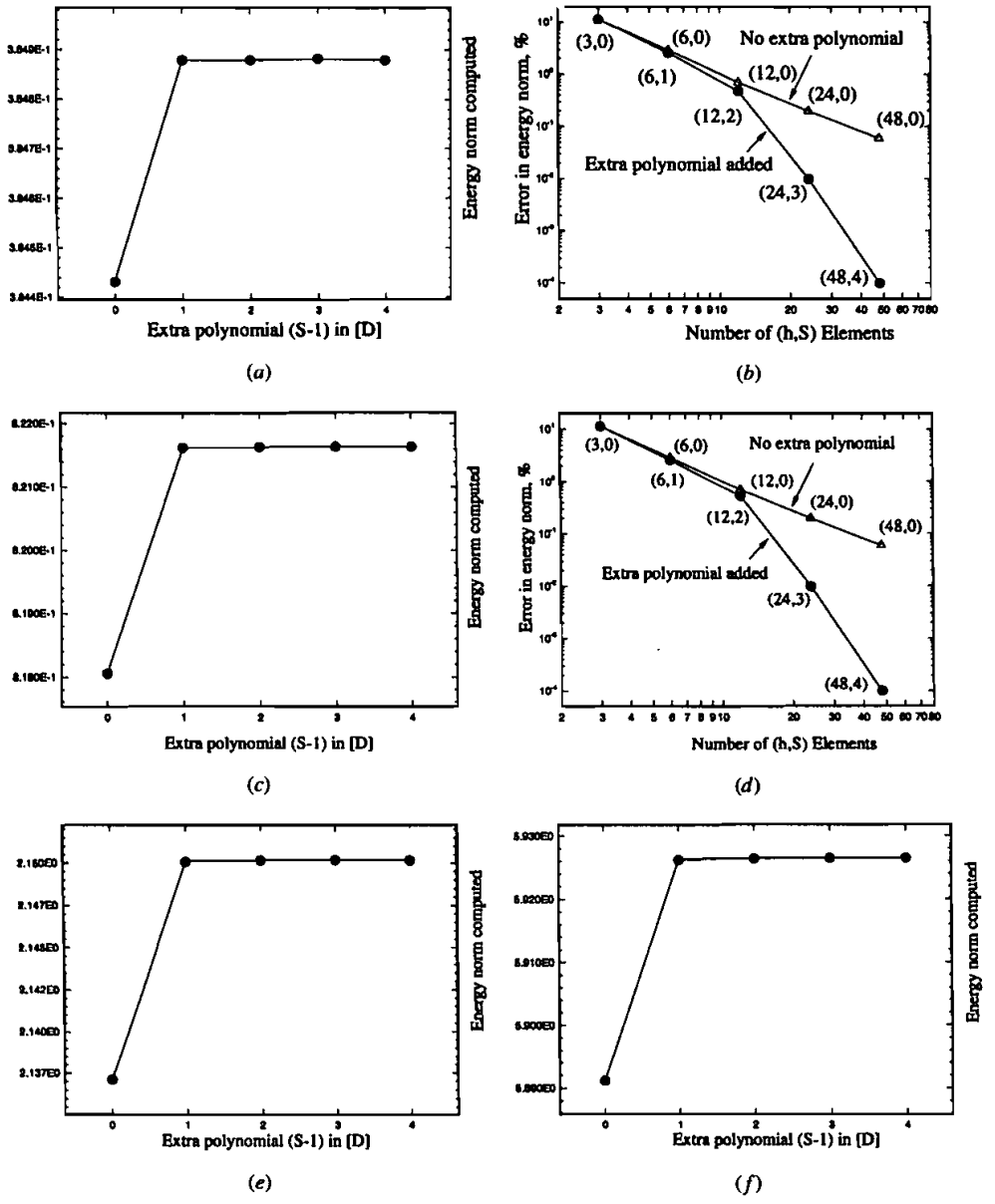

Figure 3. Effect of increasing S on solution energy in constant- and variable-source cases: (a and b) both end Dirichlet, constant source; (c and d); both end Dirichlet, variable source; (e) left end Dirichlet, right end Neumann, constant source ($s = 1$); (f) left end Dirichlet, right end Neumann, variable source ($s = \rho$).

where $\mathrm{Pe} = u\ell/\epsilon$ is the model problem "Peclet number." Solutions to (49) are thus parameterized by Pe. For Dirichlet boundary conditions $q(0) = 0$ and $q(1) = 1$, the analytical solution to (49) is

$$q(x) = \frac{e^{x\,\mathrm{Pe}} - 1}{e^{\mathrm{Pe}} - 1} \tag{50}$$

which exhibits a sharp thin-layer character dependent on Pe. Further, via (39), the analytical solution energy seminorm is $\|q\|_E = 0.25(e^{\mathrm{Pe}} + 1)/(e^{\mathrm{Pe}} - 1)$, which converges to exactly $\|q\|_E = 0.25$ as $\mathrm{Pe} \to \infty$. Finally, the associated endpoint boundary fluxes for (50) equal exactly zero and unity.

In practical CFD situations, Pe can range to 10^5. Accurately resolving such a solution numerically requires local fine meshing, and/or artificial diffusion, and the dominant error mechanism is dispersive. This is clearly illustrated in Figures 4*a* and 4*b* for the Lagrange $k = 1$ and $k = 2$ Galerkin WS solutions on a uniform Nnode = 13 mesh for $\mathrm{Pe} = 10^3$. A nonuniform 13-node mesh can suppress the large oscillations, without added artificial diffusion, but the solution is not monotone. A uniform mesh containing 100 nodes will not yield a monotone solution for Pe = 1,000 using either the Lagrange $k = 1$ or $k = 2$ GWS algorithm.

In distinction, the optimal SGM g_2 nodeless parameter c_e yields a monotone, essentially nodally exact (to roundoff error) solution on *any* mesh, with coincident exact determination of the boundary fluxes. For example, for a uniform 13-node ($h = 1/12$) mesh using (35), the theoretically predicted value for c for a monotone solution is

$$c = \frac{U}{2}\left(\frac{3h\,\mathrm{Pe}}{2}\right) - \frac{1}{2} = \frac{1}{2}\left(\frac{3 \times 1{,}000}{2 \times 12}\right) - \frac{1}{2} = 62 \tag{51}$$

The resultant SGM g_2 solution is absolutely monotone and nodally exact to roundoff (Figure 4*c*). The energy seminorm for the computed solution is 0.25 to eight significant decimals, which exactly matches the analytical solution energy seminorm to this significance. For comparison, the SGM g_2 choice with $c = 70$, which exceeds the theoretical level, produces a diffused monotone solution, Figure 4*d*. Conversely, for $c <$ theory, the resultant SGM Solution is nonmonotone.

As another example, the appropriate c for Pe = 10,000 on a uniform five-node mesh ($h = 1/4$) is

$$c = \frac{1}{2}\left(\frac{3h\,\mathrm{Pe}}{2} - 1\right) = \frac{1}{2}\left(\frac{30{,}000}{8} - 1\right) = 1{,}874.5 \tag{52}$$

Figures 4*e* and 4*f* confirm the monotone, nodally exact SGM solutions attainable for a range of Pe for different mesh measure h_e and corresponding selection of c via (35). The WS^h-computed boundary fluxes also remain exact to roundoff.

Table 3 compares the Lagrange $k = 1, 2$ and $S = 2$ SGM g_2 element matrix for the convection-diffusion problem at Pe = 1,000. The two Lagrange basis matrices are slightly biased by the convection term, while the SGM element matrix is theoretically constructed as pure upwind to the digits shown. For Lagrange FE bases $k = 1, 2$, the diagonal terms of the system matrix approach zero as the Peclet

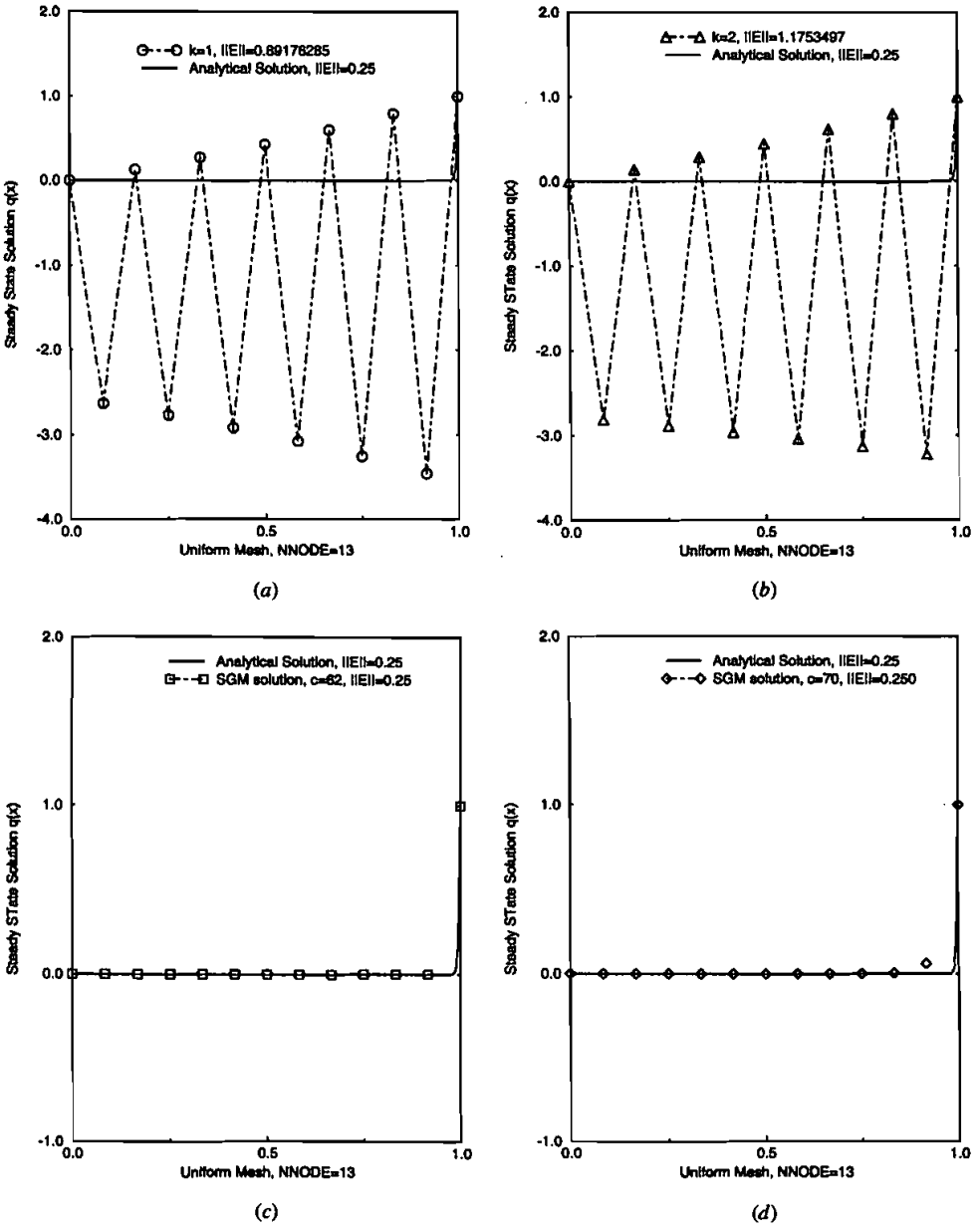

Figure 4. Verification of optimal SGM parabolic parameter c for different Pe on various meshes. (*a*) Lagrange $k = 1$, Pe = 1000; (*b*) Lagrange $k = 2$, Pe = 1000; (*c*) = SGM g_2, $c = 62$, $S = 2$, Pe = 1000; (*d*) SGM g_2, $c = 70$, $S = 2$, Pe = 1000.

number becomes large. Conversely, for this problem statement the theoretically computed SGM algorithm becomes purely upwind as Pe increases, the system matrix diagonal approaches unity. Importantly, the developed SGM theory predicts exactly the correct value for c on any mesh. Thereby, algorithm solutions can exhibit no convergence rate, since every solution is nodally exact!

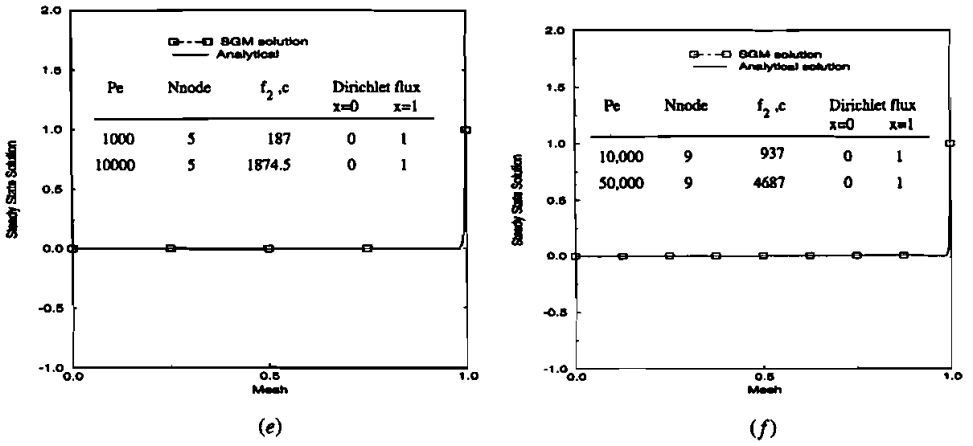

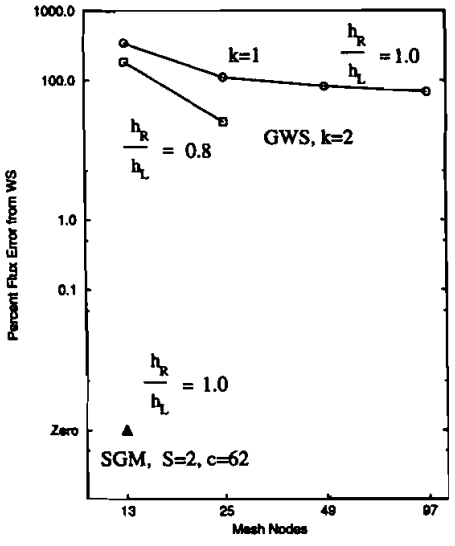

Figure 4. Verification of optimal SGM parabolic parameter c for different Pe on various meshes. (*Continued*). (*e*) SGM g_2, 5-node uniform mesh, Pe = 1000–10,000; (*f*) SGM g_2, 9-node uniform mesh, Pe = 10,000–50,000; (*g*) boundary fluxes from WS^h, Pe = 1000, $u = 1$, steady state solution.

Table 3. Comparison element matrices $[D + U]_e$, Pe = 1,000, Lagrange FE and SGM g_2

Standard GWS		SGM g_2
$k = 1\ (c = 1)$	$k = 2\ (c = 1)$	$c = 62$
$\begin{bmatrix} -0.488 & 0.488 \\ -0.512 & 0.512 \end{bmatrix}$	$\begin{bmatrix} -0.486 & 0.651 & -0.165 \\ -0.683 & 0.032 & 0.651 \\ 0.169 & -0.683 & 0.514 \end{bmatrix}$	$\begin{bmatrix} 0.000 & 0.000 \\ -1.000 & 1.000 \end{bmatrix}$

Accurate prediction of the boundary fluxes is a challenge for this problem, even if the approximate solution is nodally exact. The Lagrange FE linear and quadratic WS^h solution, for Pe = 1,000, produces a 200% error in flux even on a highly nonuniform mesh, Figure 4*g*. In distinction, for the optimal SGM, the boundary flux calculation via the weak statement is accurate to machine precision at both the left and right boundaries. Flux prediction from finite-difference formulas always have higher error than that from the WS^h, and the associated error does not decrease asymptotically unless the solution is monotone.

The velocity field for a practical problem is never a constant. This verification problem generalized for varying velocity distribution $u = mx + g$ possesses the solution

$$q(x) = e^{-h}\left[\int e^{h} r(x)\, dx + C\right] \tag{53}$$

where $h = -\int \mathrm{Pe}(mx + g)\, dx$

$$r(x) = (mx + g) - \frac{1}{\mathrm{Pe}} \frac{dq}{dx}$$

Assuming $\mathrm{Pe} \gg 1$, $(dq/dx)|_{x=0} = 0 \Rightarrow r(x) = 0$. Then, for $q(x = 0) = 0$ and $q(x = 1) = 1$, the analytical solution is

$$q(x) = \frac{e^{\mathrm{Pe}(mx^2/2 + gx)} - 1}{e^{\mathrm{Pe}(m/2 + g)} - 1} \tag{54}$$

which exhibits an even sharper wall layer than does the standard Peclet problem solution.

Specifically, for $m = -1$ and $g = 1$, $u = U = 1 - x$, (54) yields

$$q(x) = \frac{e^{\mathrm{Pe}(x - x^2/2)} - 1}{e^{\mathrm{Pe}/2} - 1} \tag{55}$$

The linear FE and $S = 2$ SGM solutions for the variable-velocity problem are compared in Figures 5*a* and 5*b* for an eight-element mesh at $\mathrm{Pe} = 10^5$. The $k = 1$ Lagrange basis solution remains oscillatory, while the $S = 2$ SGM solution is again nodally exact for the distributed SGM^h parameter distribution r_j determined from (37). Figure 5*c* confirms the SGM^h theory extension to nonuniform mesh and velocity.

Elliptic Peclet Problem, $d = 2$

The 2-D form of (48) is

$$\frac{\partial}{\partial x_j}\left(u_j q - \epsilon \frac{\partial q}{\partial x_j}\right) = 0 \qquad 1 \leqslant j \leqslant 2 \tag{56}$$

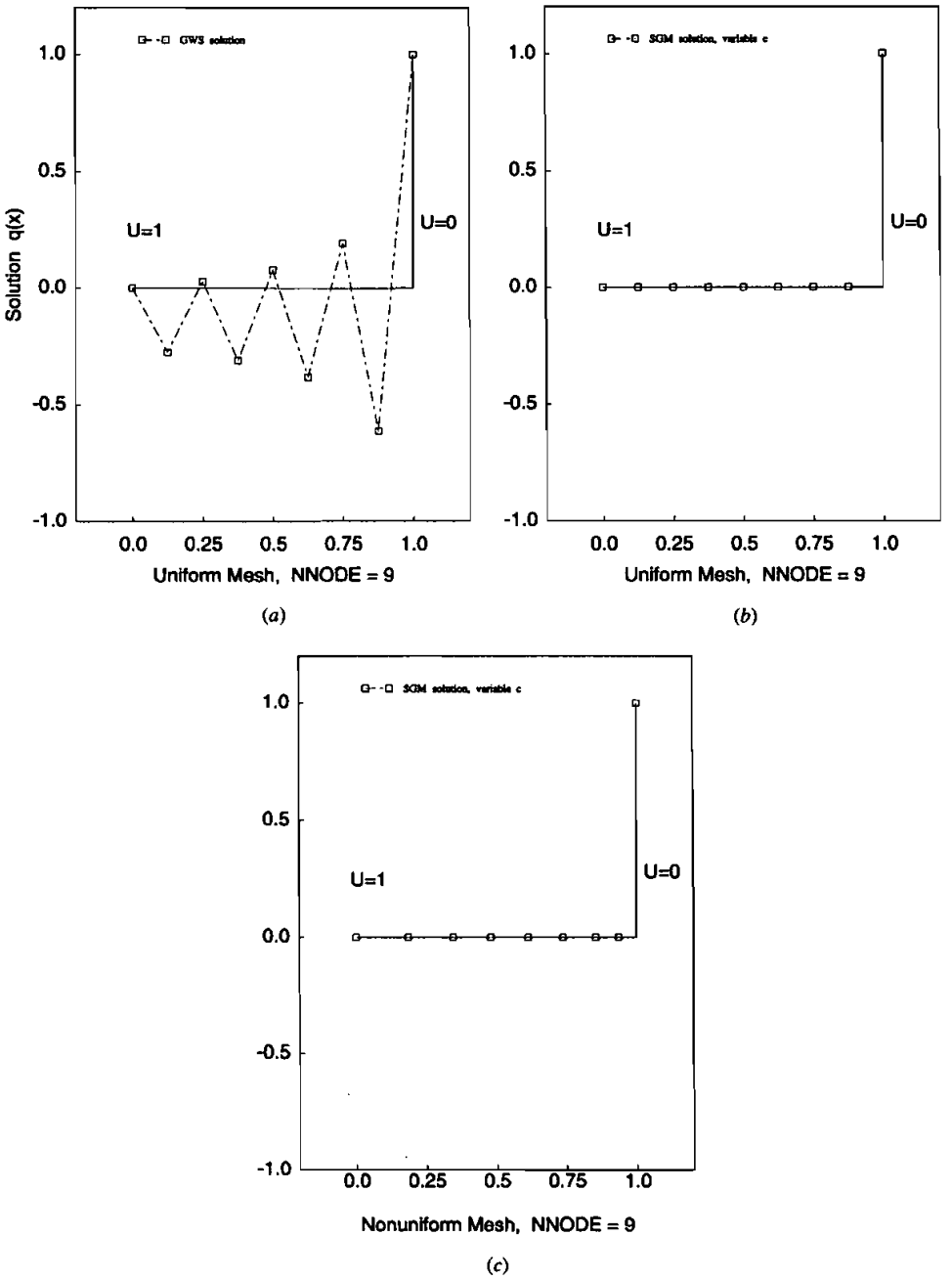

Figure 5. GWS^h and SGM algorithm solutions, Pe = 10^5, $U = (1 - x)$ verification test. (*a*) Lagrange $k = 1$ uniform Ω^h; (*b*) SGM, $S = 2$, $r_j \geqslant 1$ uniform Ω^h; (*c*) SGM, $S = 2$, $r_j \geqslant 1$ nonuniform Ω^h.

and the nondimensional analytical solution on $0 \leqslant x, y \leqslant 1$, for $u_1 = 1 = u_2$ and Dirichlet data $q(0, y) = 0 = q(x, 0)$, and $q(1, 1) = 1$, is

$$q(x) = \left[\frac{e^{x\,\mathrm{Pe}} - 1}{e^{\mathrm{Pe}} - 1}\right]\left[\frac{e^{y\,\mathrm{Pe}} - 1}{e^{\mathrm{Pe}} - 1}\right] \tag{57}$$

As $\epsilon \to 0$, i.e., Pe becomes large, the analytical solution is smooth but approaches point-singular in the near region $(x, y) \approx 1$. For Pe = 20, the exact solution (57) interpolated onto an Nnode = 13 × 13 uniform mesh is illustrated in Figure 6*a*.

The *error* distributions for the GWS Lagrange $k = 1, 2$ and the $S = 2$ SGM solutions are presented in Figures 6*b*–6*d*. The $k = 1$ solution (dispersive) error exceeds 30% in the near vicinity of (1, 1), Figure 6*b*, while the $k = 2$ error extremum in this region is nominally identical at 27%, Figure 6*c*. Thus, both Lagrange basis solutions are clearly nonmonotone on this mesh, even for the modest Pe = 20, and remain nonmonotone on mesh densities up to 50 × 50. In distinction, the $S = 2$ SGM algorithm solution with optimal $c = 1.3 = c_x = c_y$, $A = 1.2$ (numerically estimated) and $\mathscr{F}_{ij} = \mathscr{F} = 1.4$ from (38) on the 13 × 13 node uniform mesh is monotone with local error extremum of order $\sim 10^{-2}\%$, Figure 6*d*.

For Pe = 2,000 on a 9 × 9 uniform mesh, the *error* distributions for the Lagrange $k = 1$ and the $S = 2$ SGM solutions are compared in Figures 6*e* and 6*f*. The intrinsic WS dispersive error for the Lagrange basis is propagated throughout the entire domain, Figure 6*e*. Conversely, for optimal $c = c_x = c_y = 38$, $A = 0.4$ (estimated) and $\mathscr{F}_{ij} = \mathscr{F} = 9.75$ from (38), the SGM $S = 2$ solution is monotone with error extremum remaining $\mathscr{O}10^{-2}$, Figure 6*f*. Finally, the essentially nodally exact SGM g_2 solution for Pe = 20,000 on a 9 × 9 uniform mesh is shown in Figure 6*g*, as obtained for $c = 125 = c_x = c_y$, $A = 0.4$ and $\mathscr{F}_{ij} = \mathscr{F} = 30$. The extremum nodal error is again $\mathscr{O}10^{-2}$.

Linear Stationary Wave, $d = 1$

The governing PDE remains

$$u\frac{dq}{dx} - \frac{d}{dx}\left(\epsilon\frac{dq}{dx}\right) = 0 \qquad \text{on } 0 \leqslant x \leqslant \ell \tag{58}$$

Interpreting (58) as the momentum equation in system (1), the nondimensional form is

$$u\frac{dq}{dx} - \frac{d}{dx}\left(\frac{1}{\mathrm{Re}}\frac{dq}{dx}\right) = 0 \qquad \text{on } 0 \leqslant x \leqslant 1 \tag{59}$$

where Re is the Reynolds number. For Dirichlet boundary conditions $q(0) = -1$ and $q(1) = 1$, with $u(x < 0) = 1$ and $u(x > 0) = -1$, the steady-state analytical solution is

$$q(x) = \frac{1 + e^{u\,\mathrm{Re}} - 2e^{xu\,\mathrm{Re}}}{1 - e^{u\,\mathrm{Re}}} \tag{60}$$

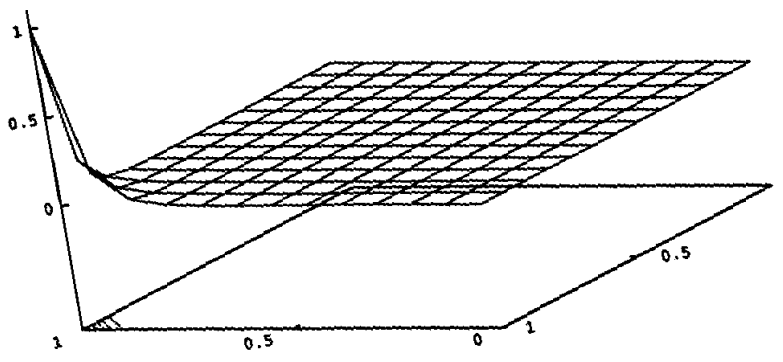

(*a*)

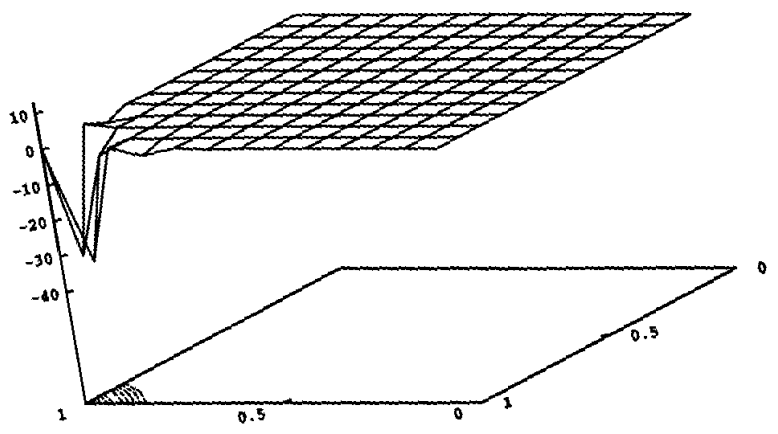

(*b*)

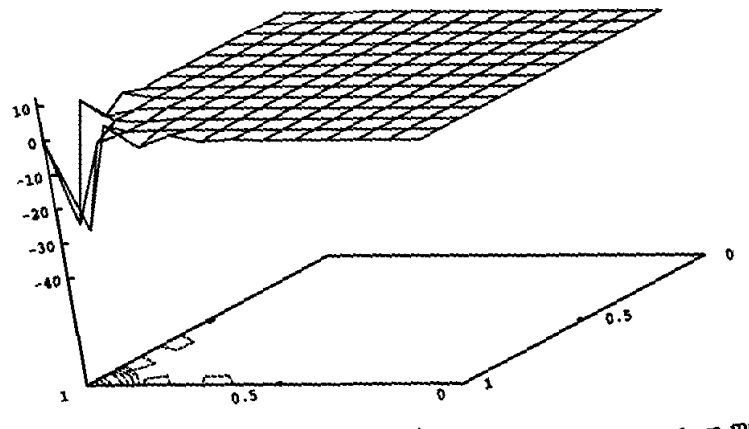

(*c*)

Figure 6. Two-dimensional elliptic Peclet problem solutions on uniform mesh: (*a*)–(*c*) Nnode = 13^2; Pe = 20. (*a*) Analyitcal solution $q(x, y)$; (*b*) error distribution, $k = 1$, (*c*) error distribution, $k = 2$.

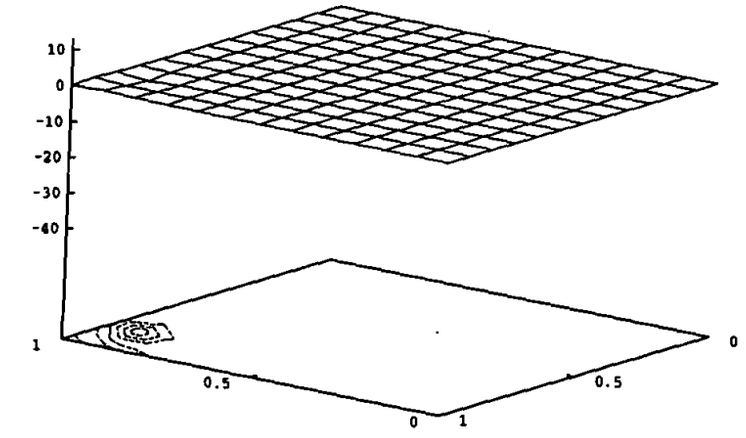

(*d*)

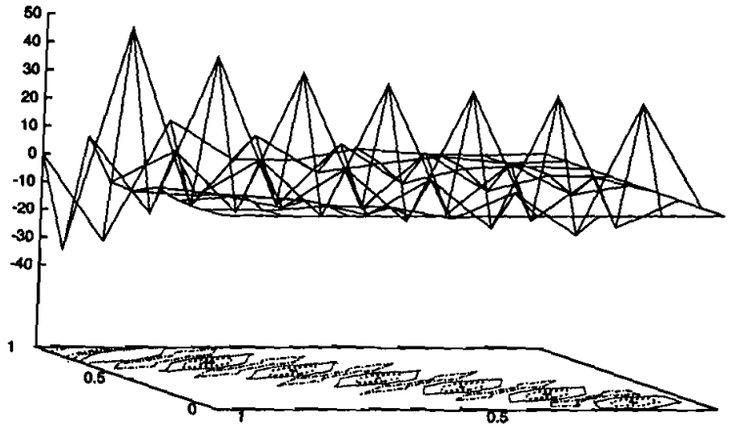

(*e*)

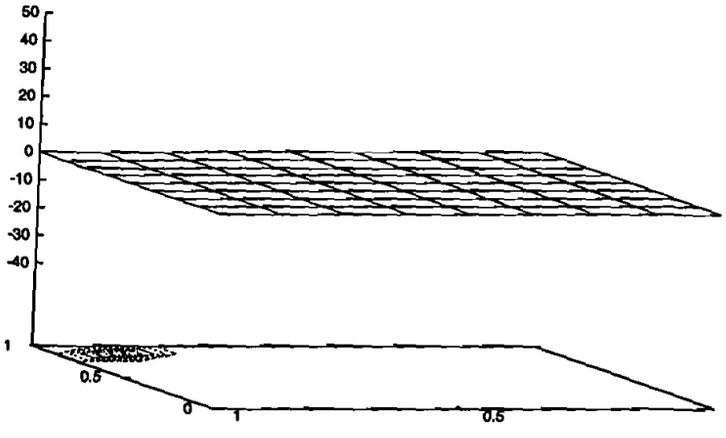

(*f*)

Figure 6. Two-dimensional elliptic Peclet problem solutions on uniform mesh (*Continued*): (*d*) Nnode = 13^2, Pe = 20, error distribution, SGM $S = 2$, $c = 1.3$, $\mathscr{F} = 1.4$. (*e*) and (*f*) Nnode = 9^2, Pe = 2,000. (*e*) Error distribution, Lagrange $k = 1$; (*f*) error distribution, SGM $S = 2$, $c = 38$, $\mathscr{F} = 9.75$.

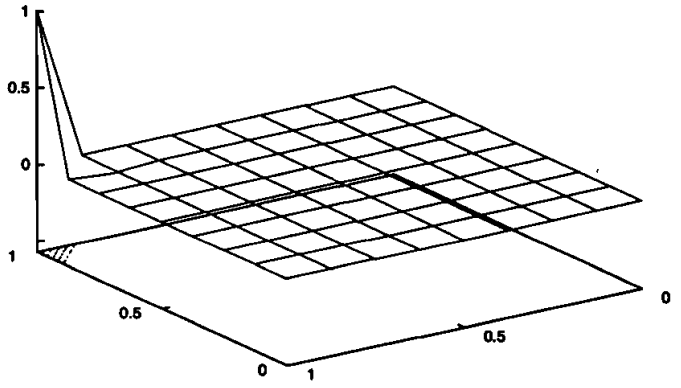

(*g*)

Figure 6. Two-dimensional elliptic Peclet problem solutions on uniform mesh (*Continued*): (*g*) Nnode = 9^2, Pe = 20,000; SGM solution, $S = 2$, $c = 124.5$, $\mathcal{F} = 30$.

Figure 7*a* graphs this a solution schematic. As Re becomes large, $q(x)$ monotonically approaches a step function with $q = 1$ behind the front trailing $u = -1$ and $q = -1$ behind the $u = 1$ front. The slope of the steady-state solution at front coalescence is

$$\frac{dq}{dx} = -\frac{2u \operatorname{Re} e^{xu \operatorname{Re}}}{1 - e^{u \operatorname{Re}}} \tag{61}$$

and as $\operatorname{Re} \to \infty$, dq/dx approaches $+\operatorname{Re}$, that is, ∞. Clearly, for large Re, the solution approaches a step function where u (nodally) changes sign.

The Lagrange $k = 1$ basis solution for $\operatorname{Re} = 10^6$ is totally oscillatory on a uniform 10-node mesh, Figure 7*d*. In fact, any Lagrange basis GWS solution will be totally dispersive on meshes up to 1,000 nodes. For this problem definition, with $\mathcal{F} = 6$ in (37), the theoretical prediction of the optimal subgrid embedding parameter corresponding to $\operatorname{Re} = 10^6$ and $h = \frac{1}{9}$ is

$$r = \frac{2c + 1}{3} = \frac{1{,}000{,}000}{6 \times 9} = 18{,}518.519 \qquad \text{hence} \qquad c = 27{,}777.278 \tag{62}$$

The resultant $S = 2$ SGM solution on the uniform 10-node mesh is absolutely monotone and nodally exact (to roundoff, 10^{-8}), Figure 7*c*.

Table 4 compares element matrices for the Lagrange $k = 1$ basis and $S = 2$ SGM basis for elements 4–6, Figure 7. The analytical-solution end fluxes for (59) are exactly zero for any $\operatorname{Re} > 1$. Any Lagrange basis solution prediction of these fluxes will be totally erroneous due to the dispersive error propagation to the Dirichlet nodes. Table 5 presents to $S = 2$ SGM WS solution for end-point fluxes, which agree to roundoff with the analytical values.

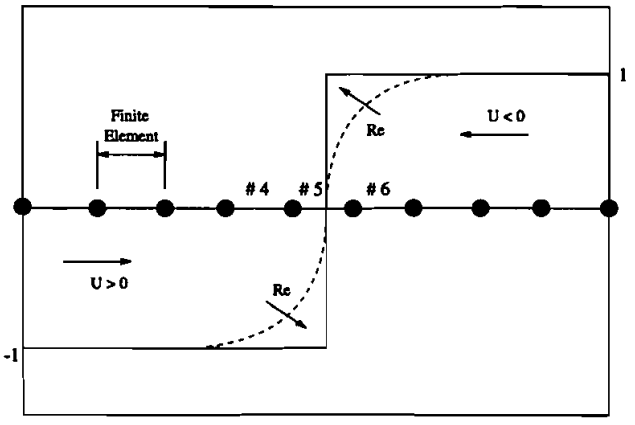

(*a*)

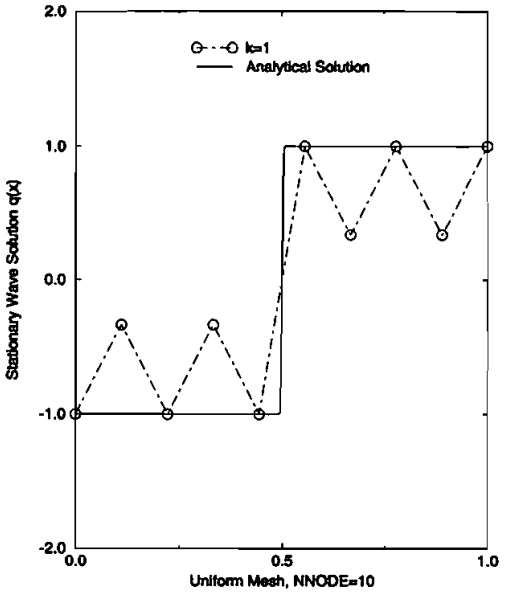

(*b*)

Figure 7. Linear square wave steady solutions on 10-node uniform mesh; (*a*) schematic wave solution, (*b*) Lagrange $k = 1$ solution.

Burgers Equation, Nonlinear Stationary Wave, $d = 1$

The nonlinear momentum variable form of (59) is the stationary viscous Burgers equation,

$$u \frac{du}{dx} - \frac{d}{dx}\left(\frac{1}{\mathrm{Re}} \frac{du}{dx}\right) = 0 \tag{63}$$

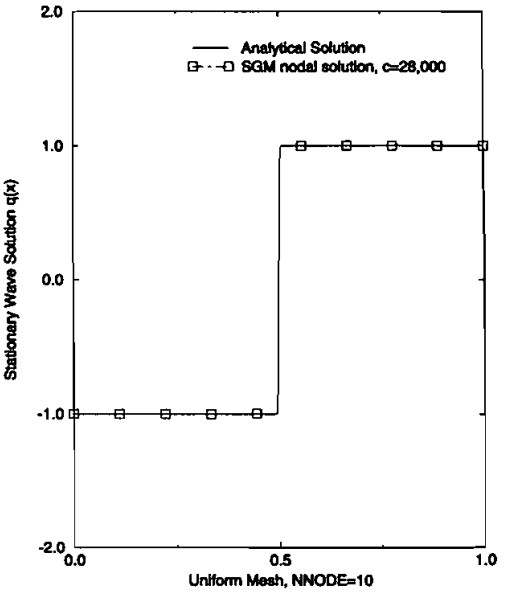

Figure 7. (*Continued*). (*c*) 10-node uniform mesh, $\mathrm{Re} = 10^6$, $S = 2$ SGM, $c = 27777.278$, $\mathscr{S} = 6$.

The weak statement algorithm (6)–(10*b*) for solution of (63) is thereby iterative. For Dirichlet boundary conditions $u = 1$ at $x = -1$, $u = -1$ at $x = 1$, and for symmetric initial data specification, the analytical solution to (63) is [17]

$$u = \tanh\left(\frac{-x\,\mathrm{Re}}{2}\right) \tag{64}$$

The analytical-solution slope at $x = 0$ thus approaches ∞ for large Re as

$$\frac{du}{dx} = -\frac{\mathrm{Re}}{2}\left(1 - \tanh^2\left(\frac{\mathrm{Re}\,x}{2}\right)\right) \quad \text{as } x \to 0, \frac{du}{dx} \text{ approaches } -\frac{\mathrm{Re}}{2} \tag{65}$$

The solution schematic, Figure 8*a*, illustrates this character.

Table 4. Example element matrices for Lagrange GWS and SGM g_2 computation

Element number see Figures 7*b* and 7*c*	Lagrange GWS	SGM g_2 (c = 27,777.278)
#4	$\frac{1}{2}\begin{bmatrix} -1 & 1 \\ -1 & 1 \end{bmatrix}$	$\frac{1}{3}\begin{bmatrix} -1 & 1 \\ -2 & 2 \end{bmatrix}$
#5	$\frac{1}{6}\begin{bmatrix} -1 & 1 \\ 1 & -1 \end{bmatrix}$	$\frac{4}{3\times 10^9}\begin{bmatrix} 1 & -1 \\ -1 & 1 \end{bmatrix}$
#6	$\frac{1}{2}\begin{bmatrix} 1 & -1 \\ 1 & -1 \end{bmatrix}$	$\frac{1}{3}\begin{bmatrix} 2 & -2 \\ 1 & -1 \end{bmatrix}$

Table 5. Boundary fluxes

Lagrange $k = 1$		$S = 2$ SGM, $c = 27{,}777.278$	
Left end, $x = 0$	Right end, $x = 1$	Left end, $x = 0$	Right end, $x = 1$
0.666986	−0.666705	$-1.6667D - 10$	$1.6667D - 10$

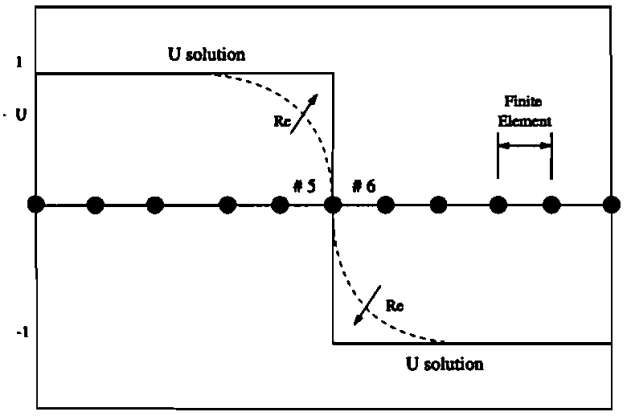

(*a*)

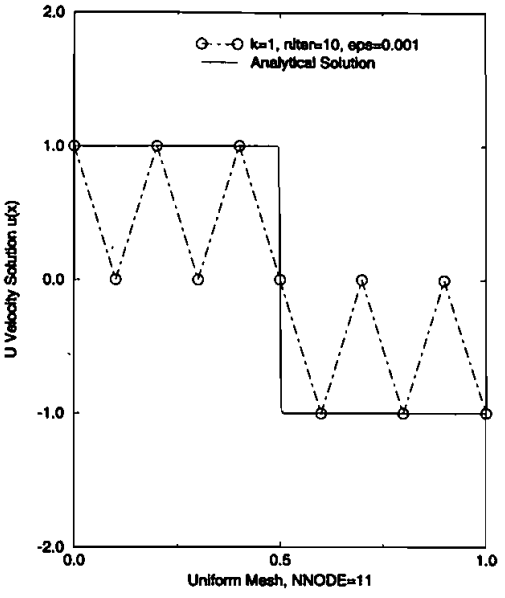

(*b*)

Figure 8. GWS and SGM solutions for nonlinear Burgers equation, Re = 100,000: (*a*) solution schematic, Nnode = 11; (*b*) $k = 1$, uniform mesh, Nnode = 11.

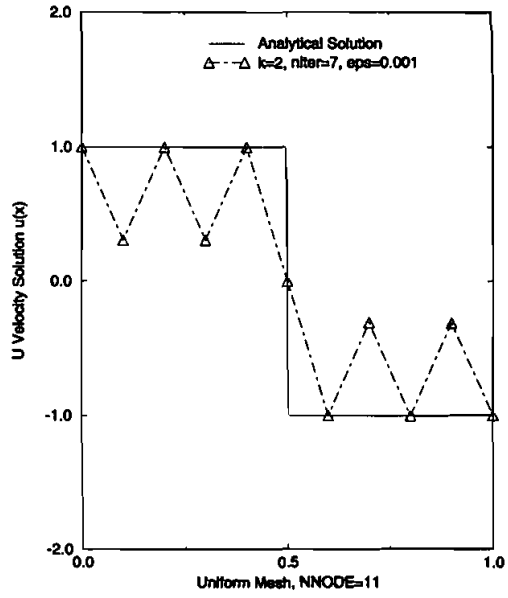

(*c*)

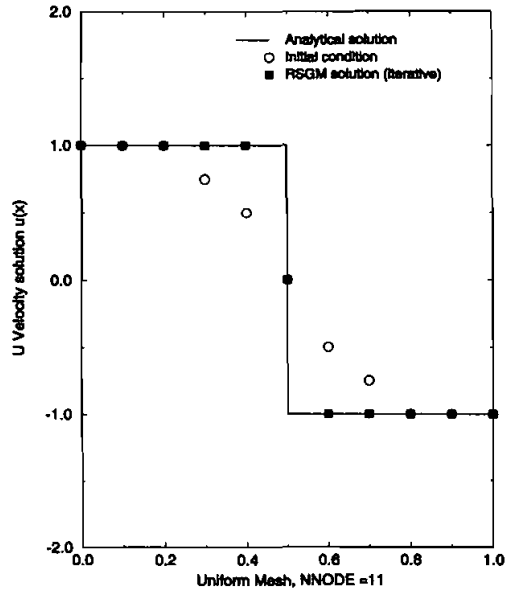

(*d*)

Figure 8. GWS and SGM solutions for nonlinear Burgers equation, Re = 100,000 (*Continued*): (*c*) $k = 2$, uniform mesh, Nnode = 11; (*d*) $S = 2$ SGM, uniform mesh, Nnode = 11.

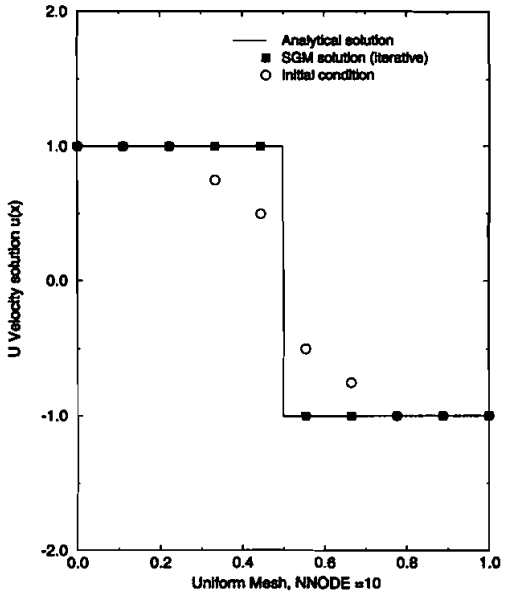

(*e*)

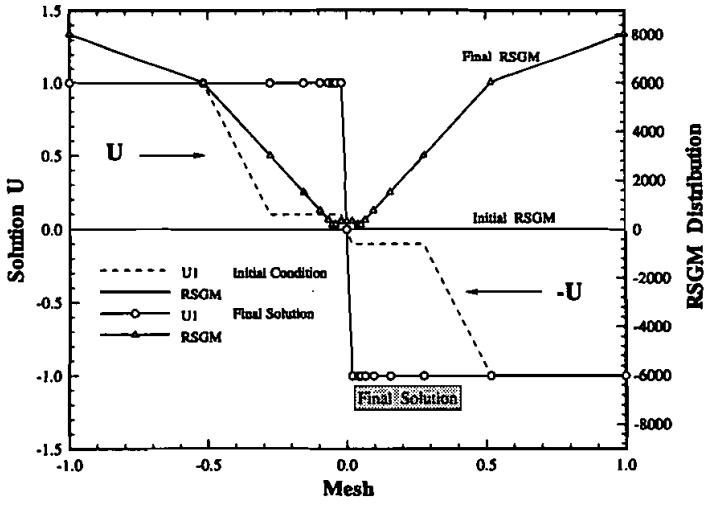

(*f*)

Figure 8. GWS and SGM solutions for nonlinear Burgers equation, Re = 100,000 (*Continued*): (*e*) $S = 2$ SGM, uniform mesh, Nnode = 10; (*f*) $S = 2$ SGM, nonuniform mesh, Nnode = 11.

Computationally, as Re becomes large, (63) moves toward becoming of hyperbolic conservation law form. The Newton iteration solution process (10*b*) for the Lagrange $k = 1, 2$ basis solution for (63) is convergent, but the dispersive error mode totally dominates the resultant nodal solution, Figures 8*b* and 8*c* for $\mathrm{Re} = 10^5$ on an 11-node uniform mesh. Although the $k = 2$ basis solution exhibits

somewhat reduced oscillation level (25%), any Lagrange basis solution on any mesh is totally unsatisfactory due to dispersive error pollution.

The nonlinear $S = 2$ SGM algorithm requires iterative determination of $c \Rightarrow c_j(u(x))$, that is, solution- and element-dependent data. Via (37):(38), the WS form of nodally distributed SGM element parameter $r_j = \{N_1\}^T\{RJ\}$ is

$$WS_e(r_j) \equiv \int_{\Omega_e} \{N_1\}\{N_1\}^T \, d\tau\{RJ\}_e - \frac{\text{Re det}_e}{\mathscr{F}} \int_{\Omega_e} \{N_1\}\{N_1\}\{N_1\}^T \, d\tau\{|U|\}_e = \{0\} \tag{66}$$

For this nonlinear solution iteration, the eigenvalue analysis for $d = 1$ confirms that $\mathscr{F} = 3$ in (37) ([17], p. 71). Verification tests were conducted with and without a $u = 0$ centroidal node on uniform meshes for the symmetric-ramp initial condition graphed as open symbols in Figures 8*d* and 8*e*. The Newton algorithm converged directly for $u = f(u, c)$, and the steady-state SGM solutions are plotted as solid symbols in Figures 8*d* and 8*e*. For the 11-node uniform mesh, the SGM solution is nodally exact, Figure 8*d*, to $\mathscr{O}(10^{-6})$, in predicting the zero node value midway in the shock. The 10-node SGM solution, Figure 8*e*, is nodally exact to $\mathscr{O}(10^{-8})$ without the mid-shock node.

Table 6 compares the Lagrange and SGM element matrices in the region where the analytical solution changes sign (elements 5 and 6, Figure 8*a*) for Newton iterations 1 and 6. The SGM element parameter $r_j = r_j(u_j, h_e, \text{Re})$ is computed at each node j during the iterative process. Finally, for a highly nonuniform mesh, attracted to the shock location, the SGM nodal solution, and the corresponding initial and final computed distribution of the SGM parameter r_j, are shown in Figure 8*f*. The SGM solution is monotone and essentially nodally exact to $\mathscr{O}(10^{-8})$, and $r_j(u_j, h_e)$ spans the range $\pm 10^4$, dependent on both h_e and u_j.

Gaussian Plume, Directional Diffusion in a Convective Field, $d = 3$

The standard benchmark problem ([19], chap. 4.12) calls for prediction of the steady-state convective-diffusive transport of a neutrally buoyant contaminant introduced into a directional uniform velocity field in three dimensions. The

Table 6. Element matrices for Burgers equation algorithms, 11-node mesh, Re = 10^5

Elem. no.	Iter. no.	Lagrange $k = 1$	SGM $S = 2$	Comments
5	1	$\begin{bmatrix} -0.167 & 0.167 \\ -0.083 & 0.083 \end{bmatrix}$	$\begin{bmatrix} 0.166678 & -0.166678 \\ -0.416678 & 0.416678 \end{bmatrix}$	GWS matrices are not positive semidefinite
6	1	$\begin{bmatrix} 0.083 & -0.083 \\ 0.167 & -0.167 \end{bmatrix}$	$\begin{bmatrix} 0.416678 & -0.416678 \\ -0.166678 & 0.166678 \end{bmatrix}$	SGM matrices are positive semidefinite
5	6	$\begin{bmatrix} -0.325 & 0.325 \\ -0.163 & 0.163 \end{bmatrix}$	$\begin{bmatrix} 3.25D-04 & -3.25D-04 \\ -0.4999 & 0.4999 \end{bmatrix}$	GWS solution nonmonotone
6	6	$\begin{bmatrix} 0.163 & -0.163 \\ 0.325 & -0.325 \end{bmatrix}$	$\begin{bmatrix} 0.4999 & -0.4999 \\ -3.25D-04 & 3.25D-04 \end{bmatrix}$	SGM solution monotone

diffusion tensor is orthotropic with negligible component parallel to the onset flow direction. This problem was devised to verify CFD methods applied to atmospheric transport of a contaminant continuously emitted from a point source. Computationally, the "point" is distributed over a block of eight cells in a pyramidal distribution.

The governing PDE with orthotropic diffusion tensor in principal coordinates is

$$\frac{\partial q}{\partial t} + u_j \frac{\partial q}{\partial x_j} - \frac{\partial}{\partial x_i}\left(\epsilon_{(i)}\delta_{ij}\frac{\partial q}{\partial x_j}\right) - s = 0 \qquad \text{on } \Omega \times t \subseteq \mathscr{R}^3 \times \mathscr{R}^+ \qquad (67)$$

For the standard benchmark, the uniform imposed velocity field is $\mathbf{u} = 1\mathbf{i} + 0\mathbf{j} + 0\mathbf{k}$ with $\epsilon_1 = 0$, $\epsilon_2 = 0.02 = \epsilon_3$. For these specifications, the Lagrange $k = 1$ and $k = 2$ WS algorithm solutions produce accurate plume prediction with modest select negative concentrations predicted about the source [19]. To better quantify dispersion error annihilation via SGM, $\mathbf{u} = 1\mathbf{i} + 1\mathbf{j} + 1\mathbf{k}$ is preferred with significantly decreased diffusion levels. Hence, $\epsilon_1 = 0.0001$, $\epsilon_2 = 0.1$, and $\epsilon_3 = 0.001$ are defined for (67).

The uniform $17 \times 17 \times 21$ standard benchmark computational mesh is retained with domain span an 80-km cube. For the modified velocity field, the source was moved to lie on the domain diagonal near the lower left domain corner. The Lagrange $k = 1$ WS algorithm steady-state solution predicts ranges of negative concentration, as shown by the "red levels" in the solution perspective, Figure *9a* (see Color Plate), with extremum -6%. The comparison $S = 2$ SGM solution, Figure *9b* (see Color Plate), is absolutely monotone, hence totally devoid of any "red levels." Elsewhere, the $k = 1$ and $S = 2$ solution fields are nominally nodally identical.

CONCLUSIONS

A subgrid embedded (SGM) finite-element basis construction has been developed, validated, and benchmarked for semidiscrete approximate constructions of a Galerkin weak statement for steady convection-diffusion applications. Element-level static condensation of the SGM-altered Lagrange $k \geqslant 2$ diffusion matrix facilitates embedding of arbitrary-degree polynomials, guaranteeing the minimal storage requirement associated with a $k = 1$ Lagrange basis algorithm.

In comparison to other theories for generating higher-order-accurate and/or monotone solutions, SGM element advantages include guaranteed (nonlinear) monotone solution with excellent conditioning of the *minimum-band* system matrix and *improved stability* via retained diagonal dominance. Further, the methodology permits retention of lexicographic ordering, for any SGM embedding, hence potentially exhibits the efficiency of strictly linear basis (or centered FD) algorithms. The verification and benchmark tests presented confirm that the SGM element solution can be guaranteed monotone via the theoretically established parameters a, b, c on arbitrary (coarse) meshes. As a weak statement adjunct, boundary fluxes computed therefrom are confirmed to be orders of magnitude more accurate than those estimated by FD or standard FE basis methods on coarse

meshes. The SGM element Galerkin weak statement algorithm has the potential to exert a fundamental impact on CFD methodology, via its intrinsic nonlinearity and guarantee of minimum computer memory and CPU requirements for high accuracy on coarse meshes in $\mathscr{P}^3$.

REFERENCES

1. A. J. Baker and J. W. Kim, *Int. J. Numer. Meth. Fluids*, vol. 7, pp. 489–520, 1987.
2. P. D. Lax, *Commun. Pure Appl. Math.*, vol. 7, pp. 159–193, 1954.
3. H. O. Kreiss and J. Lorenz, *Initial-Boundary Value Problems and the Navier-Stokes Equations*, Academic Press, New York, 1989.
4. J. P. Boris and D. L. Book, *J. Comput. Phys.*, vol. 11, pp. 38–69, 1973.
5. S. T. Salezak, *J. Comput. Phys.*, vol. 31, pp. 355–362, 1979.
6. B. Van Leer, *Proc. 8th Int. Conf. on Numerical Methods in Fluid Dynamics*, Springer-Verlag, 1982.
7. H. T. Huynh, *SIAM J. Numer. Anal.*, vol. 30, pp. 57–100, 1993.
8. I. Babuška, B. Q. Guo, and E. P. Stephan, *Math. Meth. Appl. Sci.*, vol. 12, pp. 413–427, 1990.
9. L. Demkowicz, A. Karafiat, and J. T. Oden, *Comput. Meth. Appl. Mech. Eng.*, vol. 101, pp. 251–282, 1992.
10. S. Jensen, *Comput. Meth. Appl. Mech. Eng.*, vol. 101, pp. 27–41, 1992.
11. C. Johnson and P. Hansbo, *Comput. Meth. Appl. Mech. Eng.*, vol. 101, pp. 143–181, 1992.
12. J. T. Oden, TICOM Rep. 92-09, University of Texas, Austin, TX, 1992.
13. O. C. Zienkiewicz, D. W. Kelley, J. Gago, and I. Babuska, in J. Whiteman (ed.), *The Mathematics of Finite Elements and Applications IV*, pp. 311–346, Academic Press, New York, 1982.
14. O. C. Zienkiewicz and J. Z. Zhu, *Comput. Meth. Appl. Mech. Eng.*, vol. 101, pp. 207–224, 1992.
15. J. T. Oden, *Comput. Meth. Appl. Mech. Eng.*, vol. 112, pp. 309–331, 1994.
16. T. J. R. Hughes, *Comput. Meth. Appl. Mech. Eng.*, vol. 127, pp. 387–401, 1995.
17. S. Roy, On Improved Methods for Monotone CFD Solution Accuracy, Ph.D. thesis, University of Tennessee, Knoxville, TN, 1994.
18. O. C. Zienkiewicz and A. W. Craig, in D. F. Griffiths (ed.), *The Mathematical Basis of Finite Element Methods*, Clarendon Press, Oxford, 1984.
19. A. J. Baker, *Finite Element Computational Fluid Mechanics*, Taylor & Francis, Washington, 1983.
20. S. K. Lele, *J. Comput. Phys.*, vol. 103, pp. 16–42, 1992.
21. Donoghue, W. F., *Monotone Matrix Functions and Analytic Continuation*, Springer-Verlag, Berlin, 1974.
22. J. T. Oden and J. N. Reddy, *An Introduction to the Mathematical Theory of Finite Elements*, Wiley-Interscience, New York, 1976.
23. M. B. Taylor, Private communication, 1996.

APPENDIX A: SGM ELEMENT BASIS FUNCTIONS

A basic ingredient of the SGM element, for implementation and efficiency, is static condensation [18, 19]. As the mesh is refined, with Lagrange FE methods and $k > 1$, the system degrees of freedom increase rapidly, especially in multiple dimensions. This order escallation is traced directly to (7), hence computer resource requirements for (9) increase even more rapidly. For example, in one

dimension, the global matrix is $(2k + 1)$-diagonal, and for an m-element discretization the global system is $m + 1$ rows long. For two dimensions and lexicographic ordering of the mesh, the global matrix optimum bandwidth expands to $2k(l + 1) + 1$, where l is the minimum number of nodes in either the x or y direction. In three dimensions the optimum bandwidth order is $2k((l + 1)l2 + 1) + 1$, where l is the minimum number of nodes in either the x, y, or z direction and $l2$ is the minimum number of nodes in the other two directions.

Static condensation stops escalation of matrix order for increased k and d at the element-level via element matrix rank reduction prior to global assembly. For the element residual $\{FQ\}_e$ contribution containing the product of a square matrix $[\mathrm{JAC}]_e$ of order $m^d (m > 2)$, with a column matrix q, the partitioned form is

$$\{FQ\}_{(m^d)} \equiv \begin{Bmatrix} FQ_{(2^d)} \\ FQ_{(a)} \end{Bmatrix}_{(m^d)} = [\mathrm{JAC}]_{(m^d, m^d)}\{q\}_{(m^d)}$$

$$\equiv \begin{bmatrix} \mathrm{JAC}_{(2^d, 2^d)} & \mathrm{JAC}_{(2^d, a)} \\ \mathrm{JAC}_{(a, 2^d)} & \mathrm{JAC}_{(a, a)} \end{bmatrix}_{(m^d, m^d)} \begin{Bmatrix} q_{(2^d)} \\ q_{(a)} \end{Bmatrix}_{(m^d)} \tag{68}$$

The subscripts in parentheses denote the order of the matrix. The degrees of freedom to be eliminated are contained in $\{q_{(a)}\}$, and $a = m^d - 2^d$. This is accomplished by reducing (denoted by superscript R) [JAC] to another matrix $[\mathrm{JAC}]^R$ of order 2^d via recasting (68) in the form

$$[\mathrm{JAC}]^R_{(2^d, 2^d)}\{q\}^R_{(2^d)} = \{FQ\}^R_{(2^d)} \tag{69}$$

The definitions in (68)–(69) are

$$[\mathrm{JAC}]^R_{(2^d, 2^d)} = [\mathrm{JAC}]_{(2^d, 2^d)} - [\mathrm{JAC}]_{(2^d, a)}[\mathrm{JAC}]^{-1}_{(a, a)}[\mathrm{JAC}]_{(a, 2^d)} \tag{70a}$$

$$\{FQ\}^R_{(2^d)} = \{FQ\}_{(2^d)} - [\mathrm{JAC}]_{(2^d, a)}[\mathrm{JAC}]^{-1}_{(a, a)}\{FQ\}_{(a)} \tag{70b}$$

Thereby, in (69), $a = m^d - 2^d$ degrees of freedom on Ω_e have been reduced out. In the following, we propose, only (70a) is required formed, since $\{F\}$ in (70b) vanishes for a converged solution to (9) and/or (10a–10b).

Reduction of element matrix order to the linear basis form via (70a) potentially admits selective basis degree manipulation for SGM element matrices. All higher-degree ($k > 1$) Lagrange basis functions may be chosen for condensed element diffusion matrices. However, the admissible forms are not arbitrary. Specifically, the thorough analysis documented in [17] confirms that condensation is consistent only for the diffusion matrix, $[D_k]^R_e$. The condensed mass matrix, $[M_k]^R_e$, loses normalization, while the condensed convection matrix, $[U_k]^R_e$, contains an inverse of a zero. Hence, in comparison to (7), the SGM FE semidiscrete evaluation of a Galerkin weak statement produces the modest rearrangement

$$\begin{aligned} [M] &= S_e[M_k]_e \\ \{R\} &= S_e(([U_k]_e + \epsilon_e[D_S]_e)\{Q(t)\}_e - \{b(t)\}_e) \end{aligned} \tag{71}$$

The subscript S denotes the extremum polynomial degree order of the diffusion matrix SGM embedding, while the superscript R specifies condensation operation described in (70*a*). Note that in (71) the order of all element matrices is identical. For notational simplicity, hereafter we denote $[D_k]^R$ simply as $[D_S]$.

APPENDIX B: 1-D SGM FINITE ELEMENT BASIS

In search of the SGM basis functions in one dimension (13), $\{N_S\}^T = \{N_{S_1}, N_{S_2}\}$ (say), recall Figure 1*d*, Macsyma™ (1988) is used to derive a set of integrals, via (13), that are finite and definite integrable. Selecting the SGM g_2, the final indefinite integral expressions for N_1^R and N_2^R are

$$N_{S_1}(x) = \int_{\Omega_e} \frac{|x|}{h^2}\left(-\frac{A}{B}\right)^{1/2} dx \qquad N_{S_2}(x) = \int_{\Omega_e} \frac{|x|}{h^2}\left(-\frac{C_1C_2}{D^2}\right)^{1/2} dx \tag{72}$$

where

$$\begin{aligned} A = {} & 576(c-1)^3x^8 - 3{,}456(c-1)^3hx^7 + 48(c-1)^2(175c-198)h^2x^6 \\ & - 240(c-1)^2(43c-66)h^3x^5 + 20(c-1)(320c^2 - 1{,}161c + 873)h^4x^4 \\ & - 160(c-1)(10c^2 - 75c + 81)h^5x^3 - 100(28c^2 - 90c + 63)h^6x^2 \\ & - 300(5c-6)h^7x - 225h^8 \end{aligned} \tag{73}$$

$$\begin{aligned} B = {} & 2{,}304(c-1)^2x^8 - 11{,}520(c-1)^2hx^7 + 960(c-1)(25c-27)h^2x^6 \\ & - 3{,}840(c-1)(7c-9)h^3x^5 + 80(215c^2 - 488c + 378)h^4x^4 \\ & - 1{,}200(5c^2 - 19c + 15)h^5x^3 + 300(c-6)(3c-4)h^6x^2 \\ & + 900(c-2)h^7x + 225h^8 \end{aligned} \tag{74}$$

$$C_1 = 4cx^2 - 4x^2 - 4chx + 4hx - h^2 \tag{75}$$

$$C_2 = (12cx^3 - 12x^3 - 30chx^2 + 30hx^2 + 20cxh^2 - 30xh^2 + 15h^3)^2 \tag{76}$$

$$\begin{aligned} D = {} & 48cx^4 - 48x^4 - 120chx^3 + 120hx^3 + 100ch^2x^2 \\ & - 120h^2x^2 - 30ch^3x + 60h^3x - 15h^4 \end{aligned} \tag{77}$$

Despite the complexity of these polynomials as a general function of c, for a particular c the rational fractions becomes much simpler.

Consider the $S = 2$ (that is, $k = 2$ reduced) 1-D basis function set $\{N_S\}$ as defined by (13):

$$\int_{\Omega_e} \frac{d\{N_S\}}{dx}\frac{d\{N_S\}^T}{dx}\,ds = \int_{\Omega_e} g(x,c)\frac{d\{N_{k-2}\}}{dx}\frac{d\{N_{k-2}\}^T}{dx}\,d\tau\Big|^R \tag{78}$$

The general form of 1-D SGM bases is expressed in (14) as

$$\{N_S\} = \begin{Bmatrix} 1 - \mu(\zeta) \\ \mu(\zeta) \end{Bmatrix} \tag{79}$$

For $g(x, c) = \{1, c, 1\}\{N_{k-2}\}$, the 1-D SGM matrix is given in (16). Substituting $\mu_\zeta = d\mu(\zeta)/d\zeta$, one may rewrite (78) as [23]

$$\int_{\Omega_e} \frac{d\{N_S\}}{dx} \frac{d\{N_S\}^T}{dx} dx = \frac{1}{h_e}\begin{bmatrix} 1 & -1 \\ -1 & 1 \end{bmatrix}\int_0^1 \mu_\zeta^2 \, d\zeta = \frac{2c+1}{3h_e}\begin{bmatrix} 1 & -1 \\ -1 & 1 \end{bmatrix} \tag{80}$$

Hence, μ satisfies (13) if and only if

$$\int_0^1 \mu_\zeta^2 \, d\zeta = \frac{2c+1}{3} \tag{81}$$

Let us select, $a_1 = 1$ and $a_i = 0, i \geqslant 2$ for μ in (14). Then, $\mu = \zeta^\alpha$, where α will be determined from (81) as follows:

$$\int_0^1 \left(\frac{d\zeta^\alpha}{d\zeta}\right)^2 d\zeta = \frac{2c+1}{3} \quad \text{i.e.,} \quad \frac{\alpha^2 \zeta^{2\alpha-1}}{2\alpha-1}\bigg|_0^1 = \frac{2c+1}{3} \quad \text{or}$$
$$\frac{\alpha^2}{2\alpha-1} = \frac{2c+1}{3} \equiv r \tag{82}$$

Hence, $\alpha = r \pm \sqrt{r^2 - r}$, where $r = (2c + 1)/3$. One may readily verify that $\alpha = 1$ for $c = 1$ and α becomes imaginary for $c < 1$, thus $c = 1$ is the lower limit. Examples of $\{N_S(c)\}$ are graphed in Figures 10*a* and 10*b*.

APPENDIX C: EFFECT OF c_x AND c_y IN 2-D SGM MATRICES

In higher dimensions, however, the directional influence becomes important. The aspect ratio of an element (e.g., in 2-D $\delta X/\delta Y$, Figure 10) and the directional values of c affect the ratios of the diagonal to off-diagonal terms of a diffusion matrix. A general relationship for the terms in the 2-D diffusion matrix is graphed in Figure 10. Unlike the Lagrange diffusion matrix, in the SGM diffusion matrix the ratio d_{11}/d_{13} increases as a function of $c_x c_y$ increases, Figure 10*c*. In Figure 10*d*, the comparison between the Lagrange (connected lines) and the SGM (points) diffusion matrices are documented as a function of the element aspect ratio.

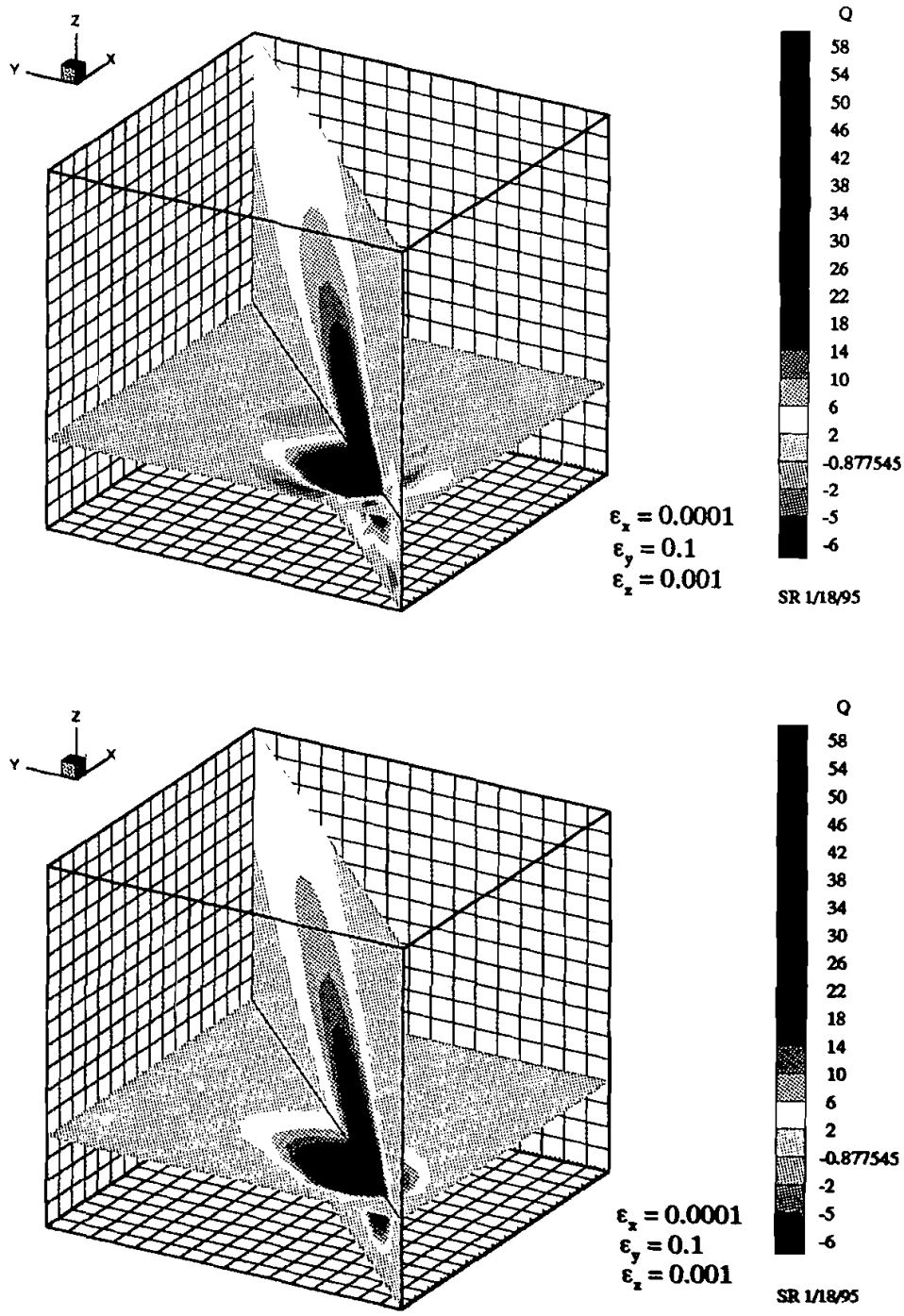

Figure 9. Three-dimensional Gaussian plume convection-diffusion solutions. (*a*) 3-D plume steady state GWS solution; (*b*) 3-D plume steady state SGM solution.

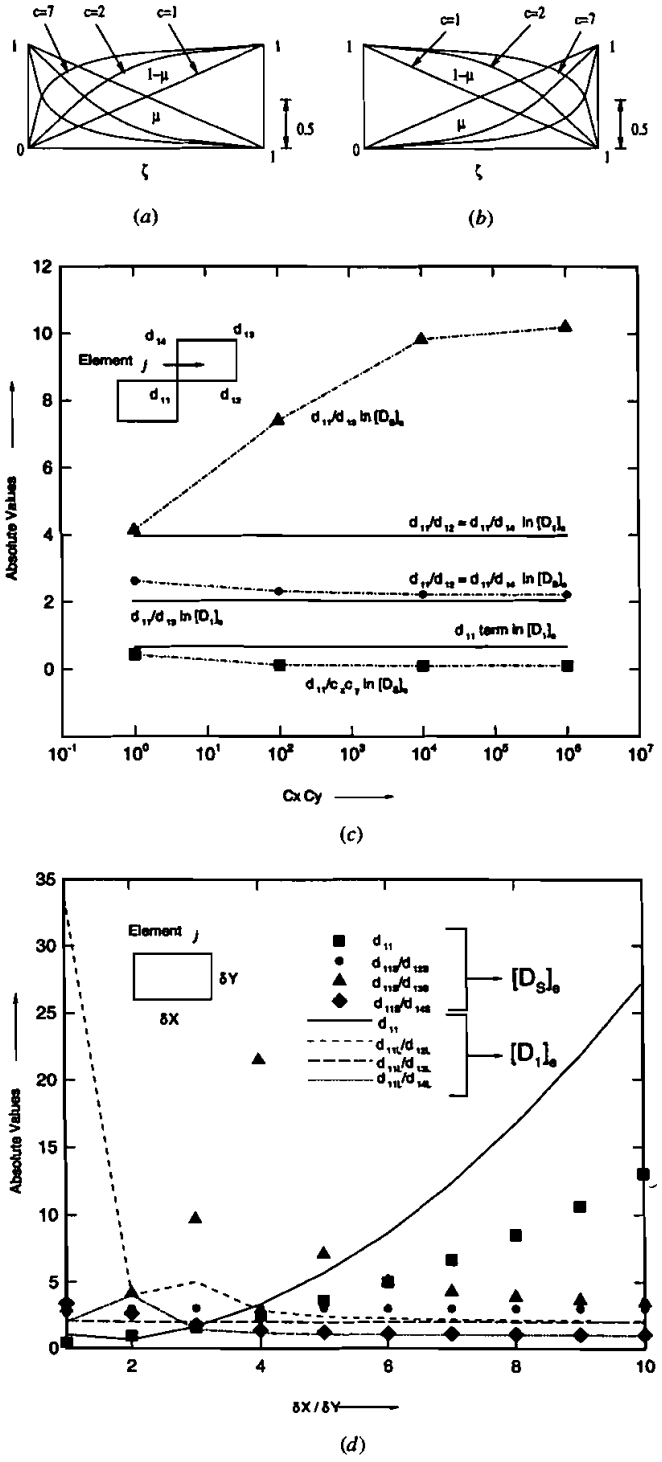

Figure 10. Comparison study of 2-D diffusion matrices, $[D_1]_e$ and $[D_S]_e$. (*a*) 1-D {*NS*}, $\alpha = r - \sqrt{r^2 - r}$; (*b*) 1-D {$N_S$}, $\alpha = r + \sqrt{r^2 - r}$; (*c*) effect of $c_x c_y$ on d_{ii}/d_{ij}; (*d*) effect of element aspect ration on $c_x c_y$.

For $c_x = c = c_y$, the SGM diffusion matrix is of the form (24) with

$$
\begin{aligned}
d_{11} &= \frac{(2c+1)(656c^3+2{,}032c^2+1{,}838c+549)}{15(148c^2+164c+73)} = d_{22} = d_{33} = d_{44} \\
d_{12} &= -\frac{(2c+1)(2c+3)(148c^2+164c+73)}{15(148c^2+164c+73)} = d_{21} = d_{23} = d_{32} \\
d_{13} &= -\frac{(2c+1)(4c+1)(16c^2+118c+111)}{15(148c^2+164c+73)} = d_{31} = d_{24} = d_{42} \\
d_{14} &= -\frac{(2c+1)(2c+3)(148c^2+164c+73)}{15(148c^2+164c+73)} = d_{41} = d_{34} = d_{43}
\end{aligned}
\tag{83}
$$

APPENDIX D: BOUNDARY FLUX COMPUTATION

In one dimension, the system matrix algebra statement for the linear form of (9) can be written as

$$
\begin{bmatrix}
b_1 & c_1 & & \mathrm{O} & \\
a_2 & b_2 & c_2 & & \\
 & & \ddots & & \\
 & & a_{J-1} & b_{J-1} & c_{J-1} \\
 & \mathrm{O} & & a_J & b_J
\end{bmatrix}
\begin{Bmatrix} Q1 \\ Q2 \\ \vdots \\ QJ-1 \\ QJ \end{Bmatrix}
=
\begin{Bmatrix} B_{x=0} \\ 0 \\ \vdots \\ 0 \\ B_{x=L} \end{Bmatrix}
\tag{84}
$$

rather than as a Newton algorithm (10*a*). While solving for the $\{Q\}$ in (84), one may enforce the Dirichlet boundary condition (say, at $x = 0$) by setting $c_1 = 0$ by setting $c_1 = 0$ and $B_{x=0} = b_1 Q_1$. Similarly, setting $a_J = 0$, $b_J = 1$, and $B_{x=L} \equiv Q_J$ in (84) will enforce a Dirichlet boundary condition at $(x = L)$ on the solution of (84) for $\{Q\}$.

Once the solution fluid $\{Q\}$ is known, the boundary fluxes corresponding to locations where Dirichlet node(s) exist may be determined in two ways. The simplest way is to use

$$
\begin{aligned}
F1 &= \left.\frac{dq}{dn}\right|_{x=0} = b_1 Q_1 + c_1 Q_2 \\
FJ &= \left.\frac{dq}{dn}\right|_{x=L} = a_J Q_{J-1} + b_J Q_J
\end{aligned}
\tag{85}
$$

Replacing (85) in (84), one may also opt for finding the (Dirichlet) boundary

flux(es) via solving the redefined system matrix algebra statement,

$$\begin{bmatrix} \frac{1}{b_1} & -\frac{c_1}{b_1} & & \circ & \\ \frac{a_2}{b_1} & \left(b_2 - \frac{a_2 c_1}{b_1}\right) & c_2 & & \\ & & \ddots & & \\ & & a_{J-1} & \left(b_{J-1} - \frac{c_{J-1}a_J}{b_J}\right) & \frac{c_{J-1}}{b_J} \\ & \circ & & -\frac{a_J}{b_J} & \frac{1}{b_J} \end{bmatrix} \begin{Bmatrix} F1 \\ Q2 \\ \vdots \\ QJ-1 \\ FJ \end{Bmatrix} = \begin{Bmatrix} Q_1 \\ 0 \\ \vdots \\ 0 \\ Q_J \end{Bmatrix} \tag{86}$$

Note in (86) that both ends of the domain are considered as containing Dirichlet boundary data.

In general, therefore, the direct flux computation at nodes on a dirichlet boundary can be done via the following matrix product:

$$[J]\{Q\} = \{\text{flux}\} \tag{87}$$

where Q is the final solution for a d-dimensional problem statement and $[J]$ is the decoupled, full-dimensional Jacobian formed for each particular dependent variable.